Influence of the Tian Shan on Arid Extratropical Asia

JANE BALDWIN

Princeton University, Princeton, New Jersey

GABRIEL VECCHI

Geophysical Fluid Dynamics Laboratory, Princeton, New Jersey

(Manuscript received 16 July 2015, in final form 2 May 2016)

ABSTRACT

Arid extratropical Asia (AEA) is bisected at the wetter Tian Shan (a northern offshoot of the Tibetan Plateau) into east and west deserts, each with unique climatological characteristics. The east deserts (~35°–55°N, ~75°–115°E) have a summer precipitation maximum, and the west deserts (~35°–55°N, ~45°–75°E) have a winter–spring precipitation maximum. A new high-resolution (50 km atmosphere–land) global coupled climate model is run with the Tian Shan removed to determine whether these mountains are responsible for the climatological east–west differentiation of AEA. Multicentennial simulations for the Control and NoTianshan runs highlight statistically significant effects of the Tian Shan. Overall, the Tian Shan are found to enhance the precipitation seasonality gradient across AEA, mostly through altering the east deserts. The Tian Shan dramatically change the precipitation seasonality of the Taklimakan Desert directly to its east (the driest part of AEA) by blocking west winter precipitation, enhancing subsidence over this region, and increasing east summer precipitation. The Tian Shan increase east summer precipitation through two mechanisms: 1) orographic precipitation, which is greatest on the eastern edge of the Tian Shan in summer, and 2) remote enhancement of the East Asian summer monsoon through alteration of the larger-scale seasonal mean atmospheric circulation. The decrease in east winter precipitation also generates remote warming of the Altai and Kunlun Shan, mountains northeast and southeast of the Tian Shan, respectively, due to reduction of snow cover and corresponding albedo decrease.

1. Introduction

There are a number of large-scale arid regions in the world, and most of them are in the subtropics. The arid regions in interior Asia are vast and unique. Spanning roughly 45°–115°E and 35°–55°N, these arid lands are located farther into the extratropics than any other major desert, excluding the far polar latitudes (Fig. 1). The Tibetan Plateau along with the related orography, which exists on the periphery of these deserts, plays a number of key roles in shaping this climate, creating local rain shadow and remote monsoon effects (Molnar et al. 2010; Broccoli and Manabe 1992; Rodwell and Hoskins 1996). The highest mountain range within arid extratropical Asia (AEA) is the Tian Shan, which extend northwest of the Tibetan Plateau and reach 7439 m at the highest peak (Fig. 2a). In the present climate, AEA is meridionally bisected into west and east deserts by a relatively wet area centered near 75°E that is collocated with the Tian Shan (Figs. 3a,b). These macrodeserts are composed of a number of smaller named deserts, including the Kyzyl Kum and Kara-Kum in the west and the Taklimakan and Gobi Deserts in the east, among others. Their land surface ranges from grass-covered steppe, to sand dunes, to gravel (Yang et al. 2011; Zonn and Esenov 2012; Lioubimtseva et al. 2005).

In this chronically water-stressed region of the world, slight variations in precipitation and land use can cause large fluctuations in desert extent (Yu et al. 2004), potentially magnified through vegetation feedbacks (Charney 1975). These desert variations in turn significantly impact agriculture and natural vegetation (Ososkova et al. 2000; Bai et al. 2008; Do and Kang 2014). Given that the east deserts are a primary source of dust in the atmosphere, these variations can have impacts far afield from AEA as

Corresponding author address: Jane Baldwin, Program in Atmospheric and Oceanic Sciences, Princeton University, 201 Forrestal Rd., Princeton, NJ 08540.
E-mail: janewb@princeton.edu

DOI: 10.1175/JCLI-D-15-0490.1

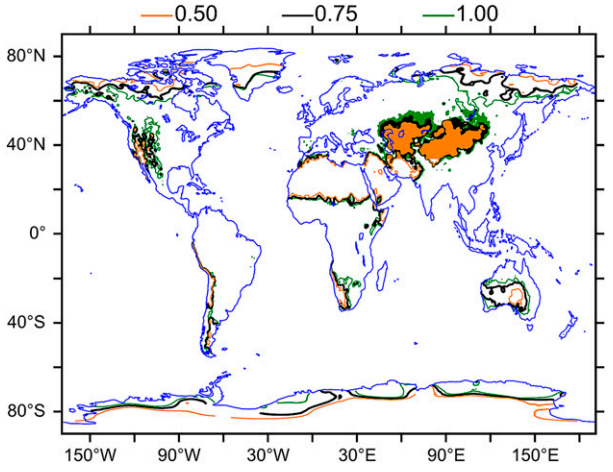

FIG. 1. Arid places globally, with AEA shaded. Desert area is determined with three different annual mean precipitation thresholds (<0.50, <0.75, or <1.00 mm day^{-1}) applied to the University of Delaware precipitation dataset. Note that the deserts in extratropical Asia are the only major extratropical deserts, excluding the far polar regions.

well (Qian et al. 2002; Zhang et al. 2003; Wang et al. 2004). As a result, understanding sources and variability of moisture in AEA is a critical challenge.

Water isotope measurements (Aizen et al. 1996; Araguás-Araguás et al. 1998; Kreutz et al. 2003; Aizen et al. 2006) and modeling approaches (van der Ent et al. 2010; Sun and Wang 2013; Barnes et al. 2014) have been used to track water into this continental region. These studies suggest a number of moisture sources for this region. Moisture follows the westerlies from the Caspian, Aral, Mediterranean, and Black Seas as well as the Atlantic Ocean all the way to AEA, particularly the west deserts. Monsoonal circulations from the Pacific and Indian Oceans also provide a source of precipitation, especially for the east deserts. Moisture carried by the westerlies tends to travel farther than monsoonal moisture, with the east deserts receiving more moisture recycled through the land surface than the west deserts. Interannual precipitation variability in these regions reflects variability in these moisture sources; in particular, the North Atlantic Oscillation and monsoon variability have been shown to modulate precipitation in the east deserts (Yatagai and Yasunari 1995; Aizen et al. 2001; Schiemann et al. 2009; Linderholm et al. 2011). Related to these different predominant moisture sources, there is a gradient in seasonality of precipitation across AEA, with precipitation peaking in winter–spring in the west deserts and summer in the east deserts (Fig. 4). Mountain glacier melt, especially from the Tian Shan, provides a key water resource that allows some resilience against these seasonal and interannual precipitation variations (Aizen and Aizen 1997; Aizen 2011).

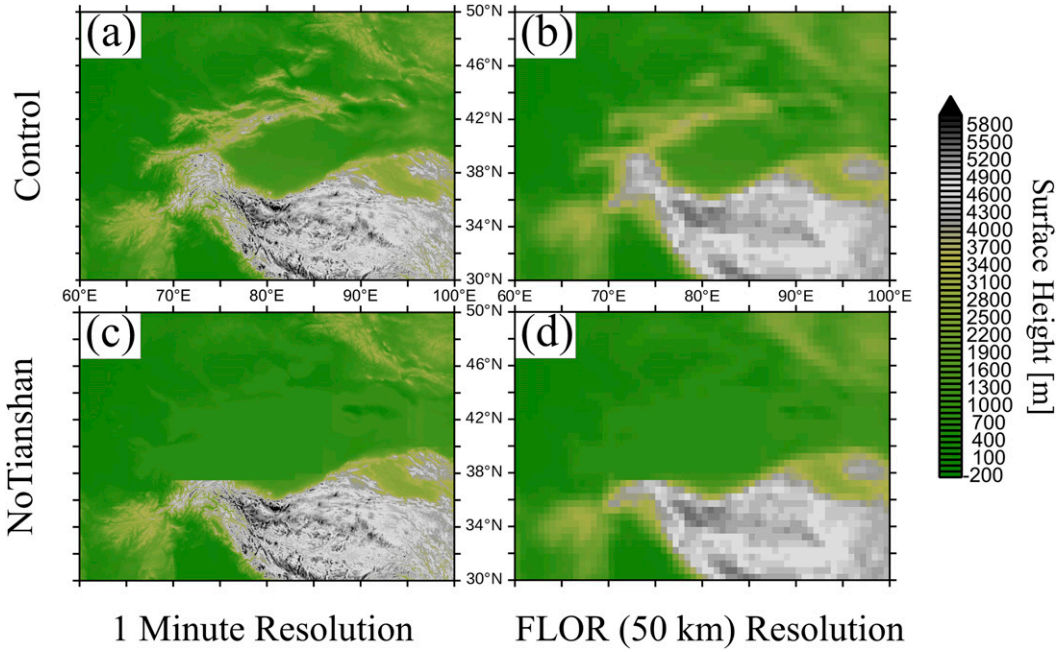

FIG. 2. Elevation in AEA for Control and NoTianshan. (a),(c) High-resolution observed topography (USGS 1′ digital elevation model). (b),(d) FLOR's 50-km-resolution surface height boundary conditions. Comparison of (a) and (b) demonstrates the accuracy of FLOR's topography. Comparison of (a),(b) vs (c),(d) demonstrates where the Tian Shan were flattened in model simulations.

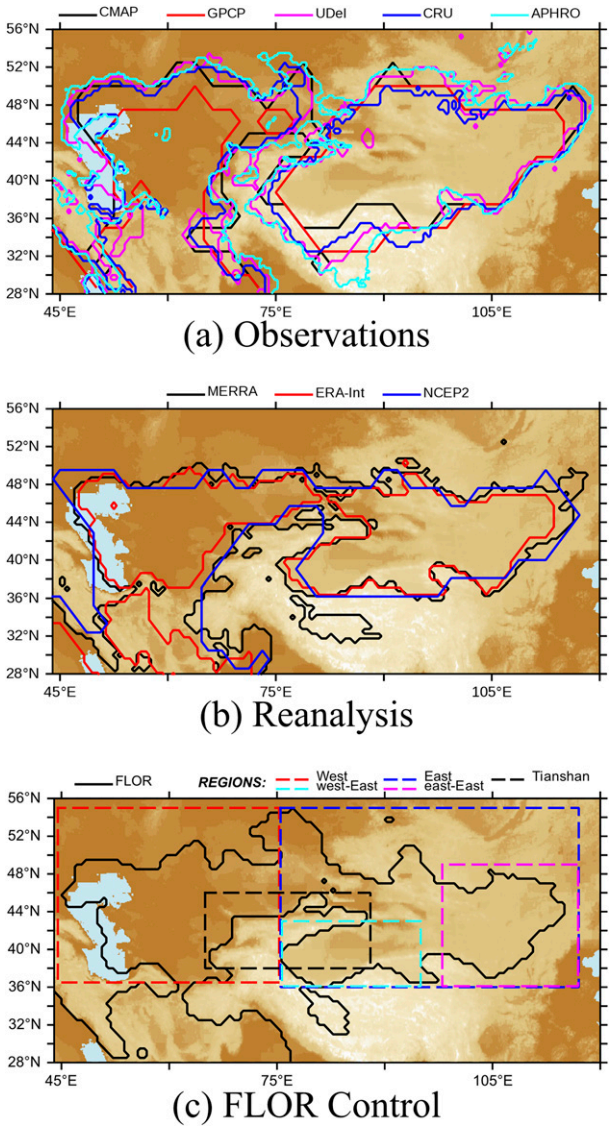

FIG. 3. Observed vs simulated area of AEA and subregions examined in this study. ETOPO5 topography (shaded) is overlaid with outlines of deserts (annual mean precipitation $<0.75\,\text{mm day}^{-1}$) according to (a) precipitation observed from satellites and ground-based measurements, (b) precipitation from reanalysis, and (c) precipitation from the FLOR Control run. Boxes in (c) designate particular regions examined in this analysis (i.e., west deserts, east deserts, western-east region, and eastern-east region). Regional seasonal cycles are calculated by averaging over only desert points within the region's box, excluding major inland lakes and seas, except for the Tian Shan region where only nondesert points are averaged over.

Beyond interannual time scales, distant past and more recent environmental changes in AEA have been dramatic. Paleoclimatic evidence indicates that this region first became arid around 20–40 million years ago (Myr), corresponding with a combination of Tibetan Plateau uplift, global cooling, and retreat of the inland extending Paratethys sea (Rea et al. 1998; Guo et al. 2002; Dupont-Nivet et al. 2007; Bosboom et al. 2014). At a smaller scale, the uplift from the Tian Shan was likely simultaneous with, and caused, development of the Taklimakan Desert (Zheng et al. 2015). Over the last Quaternary period (last 2 Myr), the deserts have been quite dynamic, with pluvials and droughts since the start of the Holocene (11 700 years ago) implicated in the rise and fall of numerous civilizations (Yang et al. 2006, 2011; Pederson et al. 2013, 2014). Over this same period, an out-of-phase relationship has been documented between precipitation in monsoonal Asia and the east deserts of AEA, which is tied to variations in Earth's orbit and insolation (Herzschuh 2006; Chen et al. 2008). Variations of westerly jet seasonality likely provide the tie between these insolation changes and monsoon changes (Nagashima et al. 2013; Chiang et al. 2015). Interestingly, the west and east deserts have also exhibited out-of-phase precipitation variability over the past millennium, highlighting the climatological differentiation of the regions (Chen et al. 2010).

Over the past century, both climate and land-use changes have exerted profound impacts across AEA (Groisman et al. 2009). Rising temperatures due to increasing concentration of greenhouse gases have been documented across AEA (Aizen et al. 1997; Lioubimtseva et al. 2005). This warming is paired with more precipitation but less snow and glacial mass (Aizen and Aizen 1996; Aizen et al. 1997; Hagg et al. 2007), which in turn results in greater warming at elevation through albedo decreases (Giorgi et al. 1997). Snowmelt is beginning earlier in the season, a shift that presents significant water resource challenges (Siegfried et al. 2012; Sorg et al. 2012; Unger-Shayesteh et al. 2013; Dietz et al. 2014). Related to these hydrological changes, arable land in the west deserts is predicted to not necessarily decrease but certainly shift with climate change (Bobojonov and Aw-Hassan 2014).

Simultaneous with these global warming challenges, local factors have caused significant desertification in the east and west deserts. The term desertification embodies a number of different changes including soil erosion, drying, and salinization, as well as decreases in vegetation and shifts in vegetation types (D'Odorico et al. 2013). At the edge of the east deserts, the Inner Mongolian and Mongolian steppes have become much more barren and water stressed since the 1980s, owing primarily to changes in land use, particularly overgrazing but also precipitation decrease and wind changes (Wang et al. 2006; John et al. 2009; Lu et al. 2009; Hilker et al. 2014; Li and Yang 2014). In the west deserts, the Aral Sea has decreased 74% in area and 90% in volume since the 1960s as a result of the aggressive expansion of

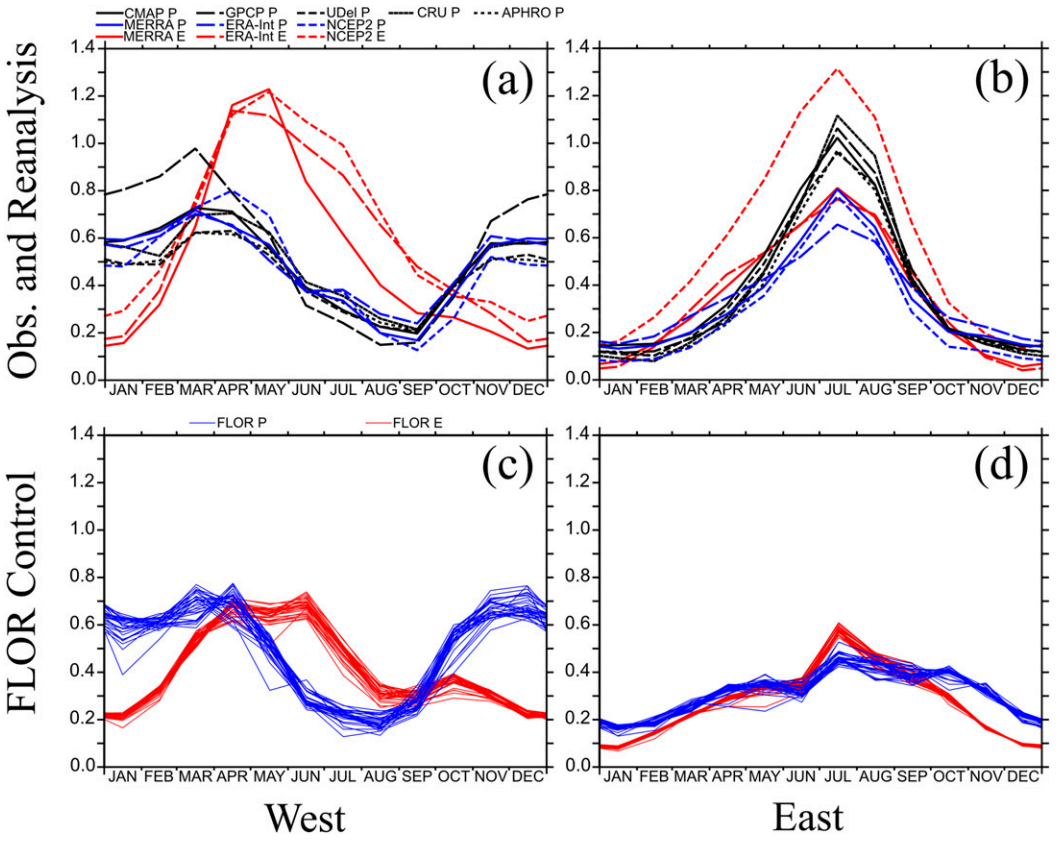

FIG. 4. Desert seasonal cycles in FLOR vs observationally derived datasets for monthly precipitation P and evaporation E (mm day^{-1}). Seasonal cycles are calculated by averaging over places in each dataset that receive <0.75 mm day^{-1} of precipitation in the annual mean, excluding major inland lakes and seas by averaging over places with elevation greater than 70 m. (left) Area-average seasonal cycles for the west deserts, and (right) the same for the east deserts. (a),(b) Seasonal cycles derived from observations and reanalysis, with gridded observed precipitation (black), reanalysis precipitation (blue), and reanalysis evaporation (red) and (c),(d) precipitation (blue) and evaporation (red) from the FLOR Control run. Each line for the model seasonal cycles is derived from 31 years of model data to match the observational and reanalysis time series length, starting every 5 years from 150 simulation years yielding 30 seasonal cycles total.

irrigation, eliminating an important water resource for the west deserts (Saiko and Zonn 2000; Micklin 2007). These environmental changes, which are unlikely to lessen as the climate continues to warm, represent significant political and policy challenges for China and Mongolia in the east and the former Soviet Union countries in the west (Parungo et al. 1994; Glantz 2005; Lioubimtseva and Henebry 2009).

Clear understanding of the basic climatic controls on AEA through modeling exercises is prerequisite to parse these recent environmental trends. Most previous modeling work relevant to AEA falls into two general categories: regional and global modeling studies. Regional modeling studies have examined subregions of AEA at a relatively high resolution using regional climate models (RCMs) or hydrological models (e.g., Small et al. 1999a,b; Xuejie et al. 2001; Sato 2005; Elguindi and Giorgi 2006; Aizen et al. 2007a,b; Sato et al. 2007; Hagg et al. 2007; Shibuo et al. 2007; Siegfried et al. 2012; Liu et al. 2014). These studies typically examine either part of the west deserts, part of the east deserts, or local orography (e.g., the Tian Shan) but not all three simultaneously. Other studies have used global climate models (GCMs) to examine Asia, in particular AEA, more broadly (e.g., Broccoli and Manabe 1992; Xue 1996; Cherchi et al. 2014). A large subset of these studies have studied the impact of the Tibetan Plateau on Asian climate using GCMs typically at around 2° latitude–longitude resolution (e.g., Manabe and Terpstra 1974; Wu et al. 2007; Wang et al. 2008; Park et al. 2010; Lee et al. 2013) with particular focus on the impact of these mountains on the South and East Asian summer monsoons (e.g., Zhisheng et al. 2001; Liu and Yin 2002; Park et al. 2012; Boos and Hurley 2013). These studies flatten the Tian Shan as part

of the Tibetan Plateau, but because of low resolution they resolve only a fraction of the Tian Shan's height and do not separate out the impact of the Tian Shan.

As noted previously, in central Asia's west deserts (Kyzyl Kum and Kara-Kum) precipitation generally peaks in the winter, while in the east deserts of China and Mongolia (Taklimakan and Gobi Deserts) precipitation generally peaks in the summer (Figs. 4a,b). Given the location of the Tian Shan between the west and east deserts, the question arises: Are the Tian Shan responsible for both the spatial and seasonal division of AEA? Until recently, only one prior modeling study (Sato 2005) had focused on the climatic impact of the Tian Shan specifically, simulating 10 years with the Tian Shan removed in a 150-km-resolution regional climate model. This study found that the Tian Shan do not significantly change the annual mean aridity of AEA but did not explore seasonal precipitation changes. Paleoclimate proxies indicating the asynchronous uplift of different parts of the Tibetan Plateau have recently spurred a handful of additional studies examining the contrasting impacts on Asian climate of different parts of the Tibetan Plateau. These studies include experiments with regional climate models over Asia with resolutions of 50 km and 1° (Tang et al. 2013; Liu et al. 2015) and an approximately 2° resolution global atmospheric model forced with climatological SSTs (Zhang et al. 2012). Notably, all three studies find an enhancement of the East Asian summer monsoon by the northern Tibetan Plateau, which includes the Tian Shan; Liu et al. (2015) also highlight the drying of the Tarim basin, which is where the Taklimakan Desert exists in the present climate, by this orography.

The present study revisits this question of Tian Shan climatic influence with a more accurate model and new focus on precipitation seasonality differences across AEA. We employ GFDL's newly developed higher-resolution (50 km atmosphere–land) forecast-oriented low-resolution version of CM2.5 (CM2.5-FLOR, hereafter FLOR) to simulate global climate with and without the Tian Shan and explore the Tian Shan's influence on AEA. Similar to regional models, FLOR simulates Tian Shan topography and desert borders with fidelity. However, using a coupled atmosphere–ocean global model also allows exploration of remote atmospheric influences of orography (e.g., stationary waves; Hoskins and Karoly 1981) and interaction with oceans, both of which have been shown to be important for monsoons. In summary, the goal of this paper is to employ high-resolution GCM simulations to assess the role of the Tian Shan in creating the differing characteristics of the east and west deserts of AEA. The rest of this paper is structured as follows. Section 2 describes the methods used in this study, including descriptions of observational estimates, the GCM employed (FLOR), and modeling experiment design. Section 3 compares FLOR output with observations to establish the ability of the model to simulate AEA. Section 4 describes the climatic effect of the Tian Shan on AEA as found in the modeling experiments. Section 5 concludes with a summary of the paper and discussion of the results.

2. Methods

a. Observational estimates

A significant challenge in studying AEA is the relative lack of observations in this sparsely populated region. The approach taken in this study is to focus on features that are consistent among gridded global datasets, although we believe that regionally focused data products could provide crucial information. The datasets we utilize (described in more detail below) vary in the time period they cover, so we analyzed only the months common to all of the data products (January 1979–December 2009).

We analyze precipitation from five observation-based precipitation datasets (CMAP, GPCP, University of Delaware precipitation, CRU TS3.10, and APHRODITE). CMAP (Xie 2012) is a merger of five different satellite products, while GPCP (Bolvin 2012) is a merger of both satellite- and ground-based observations. Both are available at a 2.5° × 2.5° resolution. The University of Delaware precipitation and CRU time series version 3.10 (TS3.10) datasets are based on large networks of ground-based observations and are available at the relatively high-resolution of 0.5° × 0.5° (Matsuura 2010; Jones and Harris 2013). APHRODITE also merges ground-based observations but at a higher station density and only over Asia and parts of the Middle East (Yatagai et al. 2011). It is available at 0.25° × 0.25° and 0.5° × 0.5° resolution; we use the higher-resolution data in our analysis.

We also analyze precipitation and evaporation from three reanalyses (MERRA, ERA-Interim, and NCEP-2). MERRA (resolution of ½° × ⅔°; NASA GMAO 2011) and ERA-Interim (resolution of 0.75° × 0.75°; ECMWF 2009) both belong to the latest generation of atmospheric reanalyses, while NCEP-2 (resolution of approximately 2° × 2°; NOAA/NCEP 2012) is coarser resolution and an earlier product.

b. Global coupled model

In this study we employ a newly developed atmosphere–ocean coupled GFDL GCM called FLOR. FLOR features a relatively high-spatial-resolution atmosphere

TABLE 1. FLOR simulations analyzed in this study.

Simulation	Control	NoTianshan	NoTianshanDrag
Time length	200 yr (years 51–200 analyzed)	As in Control	As in Control
Radiative forcing	Year 1990	As in Control	As in Control
Vegetation	Static	As in Control	As in Control
Surface height	Standard	Tian Shan flattened	Standard
Gravity wave drag	Standard	Tian Shan flattened	Tian Shan flattened
Boundary layer roughness	Standard	Tian Shan flattened	Tian Shan flattened

and land (~50 km) and a lower-spatial-resolution ocean (1°). Compared to previous-generation GFDL coupled models such as CM2.1, which has a 1° oceanic resolution and an approximately 200-km atmospheric resolution, FLOR is better able to capture high and sharp topographic features. FLOR accounts for the primary features of the Tian Shan, as can be seen by comparing the actual topographic data in Fig. 2a with topography data smoothed to FLOR's grid in Fig. 2b. In addition to its advantages over lower-resolution models like CM2.1, FLOR has advantages compared to other recent high-resolution GCMs such as CM2.5 (50 km atmosphere–land and 0.25° ocean) in simulating the terrestrial climate of AEA. With its low-resolution ocean, multicentennial runs of FLOR are possible without excessive computational expense, allowing detection of statistically significant regional climate effects and multiple perturbation studies. FLOR is described in detail in Vecchi et al. (2014), with discussions of its skill predicting patterns of precipitation and temperature in Jia et al. (2014) and extratropical storms in Yang et al. (2015). FLOR's predecessor model CM2.5 is described in Delworth et al. (2012) and notably was found to have significantly greater skill than CM2.1 in simulating the South Asian monsoon and spatial variability of Köppen climate types.

c. Experiment design

To understand the influence of the Tian Shan on AEA's climate, we alter the topography in FLOR. Topography plays three main roles in current GFDL GCMs, including FLOR: it controls surface height, gravity wave drag, and boundary layer roughness. High-resolution boundary conditions derived from a USGS 1′ topography dataset control each of these topographic influences. Surface height is calculated by averaging this topography dataset over FLOR's 50 km × 50 km grid cells. The regridding has the side effect of smoothing the topography, reducing the height of the highest peaks (Figs. 2a,b). Gravity wave drag and boundary layer roughness are parameterized in the model as proportional to variance of the high-resolution topography dataset, averaged to the lower-resolution model grid (Pierrehumbert 1986). Additional boundary conditions in the land model, which control vegetation type and runoff flow, are also influenced by topography, but in this study we focus on the direct physical impacts of topography and leave the vegetation and hydrologic feedbacks for future work.

We utilize three different FLOR model simulations in our analysis: a control simulation (Control) and two perturbation simulations (NoTianshan and NoTianshanDrag). These simulations are described here and summarized in Table 1. Control simulates 200 years with 1990 radiative forcings, static vegetation, and standard modern-day topography in all three topographic boundary conditions (surface height, gravity wave drag, and boundary layer roughness). Only years 51–200 of the simulation are used to allow for model spinup. NoTianshan and NoTianshanDrag are identical to the Control run in all aspects except Tian Shan topography. In NoTianshan, the Tian Shan are flattened in all three topographic boundary conditions (surface height, gravity wave drag, and boundary layer roughness). In NoTianshanDrag, the Tian Shan are flattened only in boundary conditions controlling gravity wave drag and boundary layer roughness; surface height is identical to that of Control. For the perturbation experiments, the flattening is accomplished by defining an irregularly shaped region surrounding the Tian Shan and setting all elevations within that region to 800 m when the elevation is greater than 800 m (Fig. 2). The topography was set to 800 m to reflect the elevation of the surrounding landscape.

Assuming effects of perturbing different boundary conditions can be added linearly to recover their combined effect, the difference of the Control and NoTianshan simulation output (Control minus NoTianshan) is the simulated climatic influence of surface height, gravity wave drag, and boundary layer roughness from the Tian Shan, while the difference of the Control and NoTianshanDrag simulation output (Control minus NoTianshanDrag) is the simulated climatic influence of only gravity wave drag and boundary layer roughness from the Tian Shan (not surface height). The three simulations together allow analysis of how the Tian Shan affect climate and whether these

TABLE 2. Regions examined in this study. Listed spatial limits are the precise region bounds used when calculating the area-average seasonalities for Figs. 4 and 7.

Region	Longitude	Latitude	Major constituent deserts
Tian Shan	65.0°–88.0°E	38.0°–46.0°N	—
West	44.5°–75.5°E	36.5°–55.0°N	Kyzyl Kum and Kara-Kum
East	75.5°–117.0°E	36.0°–55.0°N	Gobi and Taklimakan Deserts
Western east	75.5°–95.0°E	36.0°–43.0°N	Taklimakan Desert
Eastern east	98.0°–117.0°E	36.0°–49.0°N	Gobi Desert

changes are primarily generated by the height or the drag aspects of the mountains' influence.

The long run length of 200 years (years 51–200 analyzed) was chosen to increase the signal-to-noise ratio of the results and test the robustness of remote effects of the Tian Shan, especially over East Asia. Maps of Control − NoTianshan differences represent the difference between 150-yr averages of each simulation. In Control − NoTianshan difference maps, locations are masked white where changes are not determined statistically significant at a 99% level by a two-sided Student's *t* test.

3. AEA climatology and model evaluation

The first step in exploring the climatology of AEA is choosing a definition of arid regions. One option is to use a Köppen climate classification, which combines both precipitation and temperature climatologies to estimate different climate states and has been verified for many different climate types around the globe. We explored defining arid region extent with the area of desert and semiarid land types from a Köppen climate classification scheme, using the methodology of Gnanadesikan and Stouffer (2006) to process the climate data. We also explored simpler precipitation-threshold-based definitions (e.g., locations that receive $<0.75\,\mathrm{mm\,day^{-1}}$ of precipitation). We found that the Köppen-defined AEA had similar large-scale characteristics to that of precipitation-threshold-based definitions for values of <0.5, <0.75, and $<1\,\mathrm{mm\,day^{-1}}$ of annual mean precipitation. Both types of definitions capture the major deserts of AEA, including the Kara-Kum and Kyzyl Kum among the west deserts and the Gobi and Taklimakan Deserts in the east. Both definitions also find an east–west break in aridity at the Tian Shan. Given these similarities, we employ the simpler definition; we define deserts as places that receive $<0.75\,\mathrm{mm\,day^{-1}}$ of precipitation on an annual average basis. We choose $<0.75\,\mathrm{mm\,day^{-1}}$ of precipitation as a desert definition rather than <0.5 or $<1.0\,\mathrm{mm\,day^{-1}}$ because $<0.75\,\mathrm{mm\,day^{-1}}$ creates a clear spatial differentiation between the east and west deserts (Fig. 1).

Using this definition, we examined the area of AEA in observations, reanalysis, and FLOR Control (Fig. 3). There is some variation of the desert extents between the observation and reanalysis datasets, not all of which is clearly attributable to differences in resolution. For example, the reanalyses generally indicate smaller and wetter deserts than the rain gauge– and satellite-based precipitation datasets, and ERA-Interim indicates smaller and wetter west deserts than the other reanalyses. However, all eight datasets agree that there is a collection of east deserts (including the Gobi and Taklimakan Deserts) that extend roughly from 75° to 120°E and a collection of west deserts (including the Kyzyl Kum and Kara-Kum) that extend from just beyond the Caspian Sea from about 45° to 75°E. All the datasets also collocate the wetter east–west division with the Tian Shan. FLOR Control simulates the extent of AEA generally within the range of the observed and reanalysis estimates, including distinct east and west deserts divided at the Tian Shan. Compared to the high-resolution observation datasets, FLOR's simulated east desert extent is biased small, but it is similar to that of the reanalysis. Because of its relatively high land–atmosphere resolution, FLOR also simulates boundary details only captured by the higher-resolution observation datasets (CRU TS3.10, University of Delaware precipitation, and APHRODITE) and reanalyses (MERRA and ERA-Interim).

We also examined AEA's climatology of moisture fluxes (precipitation and evaporation) in the observations, reanalysis, and model. Climatologies were computed by finding monthly average values of these quantities, averaged spatially over arid land locations (precipitation $< 0.75\,\mathrm{mm\,day^{-1}}$) in specified latitude–longitude regions (for region details see Table 2 and Fig. 3c). Major lakes, including Lake Balkash, as well as the Aral and Caspian Seas were excluded from the area averaging by selecting only places with elevation greater than 70 m. Additionally, averaging regions for the east and west deserts are truncated on the southern end around 36°N to focus on the extratropical deserts and also to remove locations on parts of the Tibetan Plateau where observations are quite sparse. For all observations and reanalyses, there is a clear pattern of precipitation peaking in the west deserts around March–April and in

the east deserts around July (Figs. 4a,b). In the east deserts evaporation peaks in the summer at the same time as precipitation, as is typical in a very dry region where evaporation is moisture limited and any moisture that reaches the ground is quickly evaporated. In contrast, in the west deserts evaporation peaks in April or May, 1 or 2 months lagged from the peak in precipitation, and remains quite substantial throughout the summer even when precipitation is at its minimum. While we are currently pursuing a related study that seeks to characterize the sources of the west deserts' dry season evaporation, the present study seeks to address whether the Tian Shan's division of the deserts is requisite for the aridity and the clear difference in seasonality of the east and west deserts.

The FLOR Control simulation accurately captures the timing of the precipitation and evaporation peaks in both the east and west deserts, including the lingering summer evaporation in the west desert (Figs. 4c,d). Notably, FLOR's accuracy in simulating the extent and precipitation–evaporation climatology of these arid regions is a significant improvement over the previous-generation model CM2.1 (not shown). Key features of FLOR versus CM2.1 that may be related to this improvement are increased atmosphere–land resolution and a more advanced version of GFDL's land model, which has deeper soil layers and more detailed vegetation.

4. Modeled climatic effects of the Tian Shan

The Tian Shan have by far their largest-magnitude effects on the local climate of Asia, with farther remote effects being too small to have much climatic significance. The magnitude of Control − NoTianshan changes was found to be much greater than that of Control − NoTianshanDrag throughout Asia, suggesting that surface height rather than gravity wave drag and boundary layer roughness dominates the climatic influence of the Tian Shan. Given these observations, the rest of our analysis focuses on comparing the Control and NoTianshan simulations in Asia, particularly AEA. These results represent the full climatic effect of the Tian Shan on this region (including gravity wave drag and boundary layer roughness) but are dominated by the influence of surface height.

a. Precipitation in AEA

There are a few ways in which the Tian Shan have a dramatic influence on precipitation in AEA (Figs. 5 and 6). First, while the Tian Shan have relatively high precipitation in Control such that there is an east–west break in the deserts, the flattened Tian Shan area is much drier, amounting to greater than 100%, up to 3 mm day^{-1} change in precipitation between the east and west deserts. This change at the Tian Shan is clearly attributable to the lack of orographic precipitation from the Tian Shan in NoTianshan. This merges the east and west deserts in the annual mean, creating a desert region in NoTianshan that appears relatively homogeneous in area extent. Next to the Tian Shan location itself, the second-greatest change in desert area is north of the Tian Shan, which is relatively dry in Control but significantly wetter in NoTianshan.

Focusing on the deserts themselves, the removal of the Tian Shan changes the west deserts very little in extent or seasonality but exerts a strong influence on precipitation in the east deserts. Interestingly, this influence varies zonally, so to describe this change, we divide the east deserts further into a western-east region, which includes the Taklimakan Desert and occupies the Tarim basin, and an eastern-east region, which includes the Gobi Desert (Table 2 and Fig. 3c). The western-east region is extremely dry all year round in Control; indeed, the Taklimakan Desert is the driest portion of AEA. In NoTianshan, this desert, while still extremely dry, receives more than twice as much precipitation in all seasons other than summer. The eastern-east region also changes but somewhat less dramatically. In Control compared to NoTianshan, winter precipitation in the eastern-east region is lower, while summer precipitation is higher. The summer precipitation increase slightly dominates the annual mean change, as the desert extends slightly less far to the east in Control versus NoTianshan.

Comparing area-average seasonal cycles of precipitation and evaporation in Control and NoTianshan highlights these changes (Fig. 7). For the west deserts, the seasonal cycles of precipitation and evaporation are almost indistinguishable in Control versus NoTianshan. The only slight change is less summer–fall precipitation and evaporation, presumably caused by eastern summer moisture being blocked by the Tian Shan. In contrast, in the east deserts there are clear changes throughout the year. The east deserts' summer precipitation peak is somewhat higher in Control compared to NoTianshan, while winter precipitation is lower. These changes are mirrored in evaporation, where summer evaporation is higher in Control compared to NoTianshan and winter evaporation is significantly lower. The east deserts' seasonality changes are magnified in the western-east region, where precipitation switches dramatically from a summer precipitation peak in Control to a much higher fall and spring double peak in NoTianshan. In contrast, in the eastern-east region the change in the summer is greater than the change in the winter, and the timing of the precipitation peak (July) does not change.

The causes of fall–spring precipitation changes in the east deserts appear to be primarily local effects. Drying

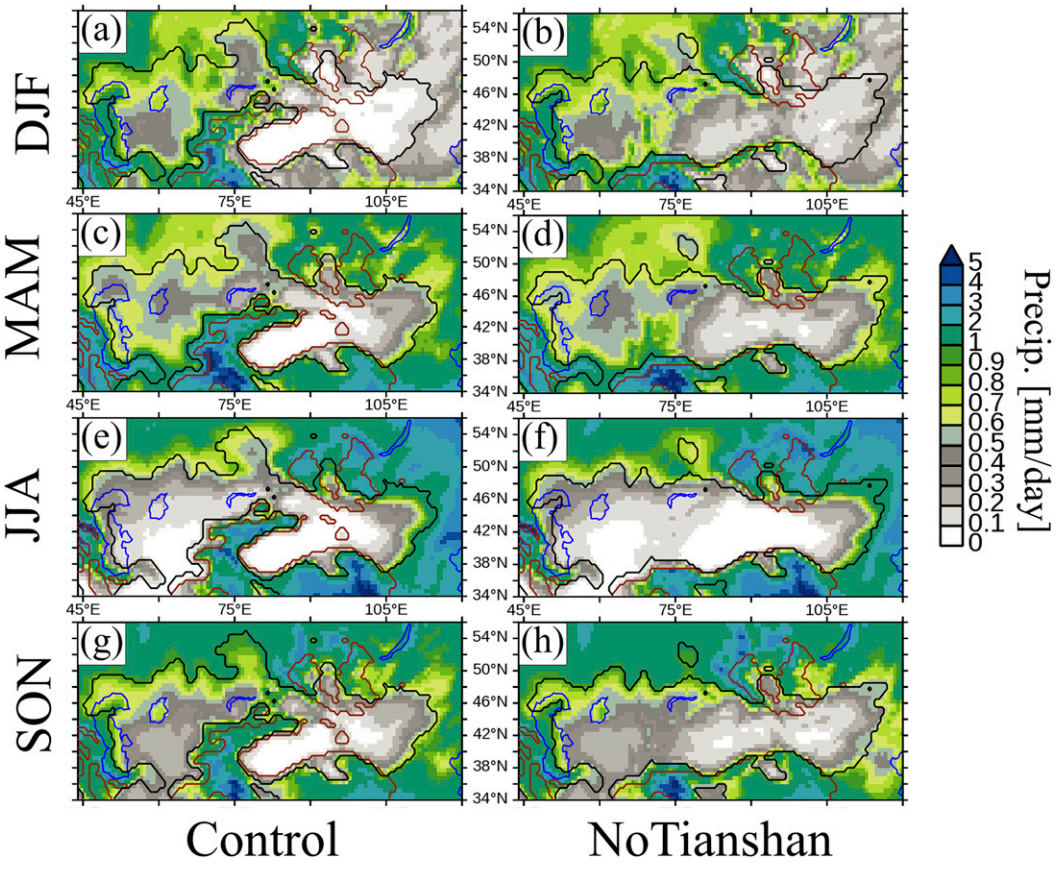

FIG. 5. Influence of the Tian Shan on seasonal mean precipitation of AEA. Precipitation is shaded for (top)–(bottom) different seasonal means and FLOR runs, (a),(c),(e),(g) Control and (b),(d),(f),(h) NoTianshan. The black contours designate the annual (not seasonal) mean desert (precipitation $< 0.75\,\text{mm day}^{-1}$) as defined for each FLOR run. The dark red contours designate places with elevation greater than 1700 m in each FLOR run's boundary conditions. The blue contours designate lakes and coastlines.

by the Tian Shan is focused directly proximal to the Tian Shan in all seasons, suggesting the high Tian Shan block moisture fluxes from differing seasonal sources (Fig. 6). In the fall to spring, meridionally averaged transects of humidity (not shown) show humidity collecting on the western side of the Tian Shan while the eastern side shows a decrease in humidity, indicating that the Tian Shan block westerly moisture fluxes from reaching the east. Further, the seasonal progression of precipitation over the Tian Shan in Control is almost identical to that of the western-east region in NoTianshan, suggesting that much of this blocked moisture is rained out as orographic precipitation over the Tian Shan (Figs. 7a,g). Orography can also generate drying through subsidence on its leeward side. Meridionally averaged transects of vertical velocity (not shown) indicate that the Tian Shan generate significant subsidence over the western-east region in winter, hardly any in summer, and intermediate amounts in spring and fall. This seasonality exists presumably because when zonal winds are stronger (as in winter), flow can go all the way up and over rather than divert around the Tian Shan. As a result of both these blocking and subsidence effects, in Control compared to NoTianshan 3 times less winter–spring precipitation occurs in the western-east region.

The implications of this winter–spring precipitation change in the western-east region are striking. Since the western-east region is extremely dry, even less than $0.5\,\text{mm day}^{-1}$ of winter–spring precipitation is enough to completely change the seasonality of this region. As a result, in the absence of the Tian Shan, the Taklimakan Desert is better characterized as a west winter–spring-precipitation desert rather than an east summer-precipitation desert. In contrast, the eastern-east region, including the Gobi Desert, retains a summer peak of precipitation even in the absence of the Tian Shan. While AEA still has zonal variation in seasonality with or without the Tian Shan, the seasonality border of the west deserts extends farther eastward when the Tian Shan are removed.

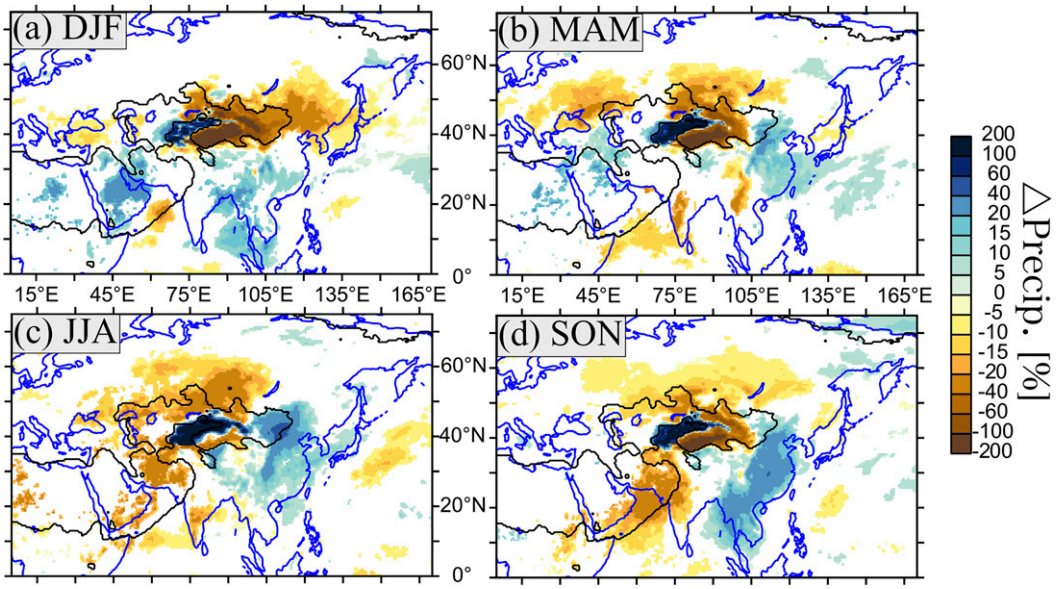

FIG. 6. Seasonal percent change in precipitation by the Tian Shan (Control minus NoTianshan). The black contour designates deserts (mean precipitation $<0.75\,\mathrm{mm\,day^{-1}}$) in the FLOR Control run. The shaded areas indicate only where there is a 99% significant difference based on a two-sided Student's t test. Percent changes are calculated by normalizing changes by the average of the Control and NoTianshan seasonal means (i.e., a change from or to zero precipitation would be a 200% change).

In addition to the winter–spring drying of the east deserts, local orographic effects also explain the slight summer precipitation increase in the western-east regions (Fig. 7g). Meridionally averaged transects of humidity indicate that around summer (but not winter) humidity builds up east of the Tian Shan, indicating that significant easterly moisture fluxes reach the Tian Shan during this season. As a result, orographic precipitation on the eastern flank of the Tian Shan is greatest in the summer (Fig. 6). This extension of orographic precipitation is primarily responsible for the slight increase in summer precipitation in the western-east region because of the Tian Shan.

In contrast to the western-east region, the eastern-east region is not directly adjacent to the Tian Shan, and its larger summer increase in precipitation cannot be explained by orographic precipitation. Control − NoTianshan differences indicate that the Tian Shan remotely generate a 20%–60% increase ($\sim$1 mm day^{-1}) in annual mean precipitation across East Asia (around 20°–55°N, 95°–135°E). While this change is statistically significant in the annual mean, it occurs from spring through fall and peaks during the summer monsoon season (Fig. 6). This enhanced East Asia precipitation has a clear influence on AEA, both increasing the summer peak in precipitation in the eastern-east region and also shortening AEA's eastern extent. As a result, it is both interesting and important to deconstruct how the Tian Shan remotely enhance precipitation in East Asia.

UNDERSTANDING REMOTE PRECIPITATION CHANGE IN EAST ASIA

A first step in understanding this East Asia precipitation enhancement is to complete a moisture budget analysis to understand whether dynamical or thermal effects drive this change. Summer change in precipitation minus evaporation ($P - E$) over this region due to the Tian Shan is positive (Fig. 8a). The value of $P - E$ is balanced by the time-averaged, column-integrated moisture flux $\mathbf{F}$ as follows from Seager and Vecchi (2010):

$$\rho_w g(P-E) = -\nabla\cdot\mathbf{F} = -\int_0^{p_s}\nabla\cdot(\overline{\mathbf{u}}\,\overline{q})\,dp - \int_0^{p_s}\nabla\cdot(\overline{\mathbf{u}'q'})\,dp - q_s\overline{\mathbf{u}}_s\cdot\nabla p_s. \quad (1)$$

Here $\mathbf{u}$ is the vector wind, and q is the humidity; p is the pressure, with p_s its surface value; g is acceleration due to gravity; and ρ_w is the density of water. Overbars indicate the monthly mean flow, and primes indicate departures from the monthly mean—that is, transient eddy quantities. The increase in $P - E$ over East Asia indicates increased moisture convergence. Different possible sources of this moisture flux are decomposed in Fig. 8b. Because of the lack of 3D high-frequency model data, the decomposition could be completed only with monthly data. Fortunately, the monthly change in moisture flux convergence from the Tian Shan $\{-[\int_0^{p_s}\nabla\cdot(\overline{\mathbf{u}}_{\mathrm{Cont}}\overline{q}_{\mathrm{Cont}})\,dp - \int_0^{p_s}\nabla\cdot(\overline{\mathbf{u}}_{\mathrm{NoT}}\overline{q}_{\mathrm{NoT}})\,dp]$, where

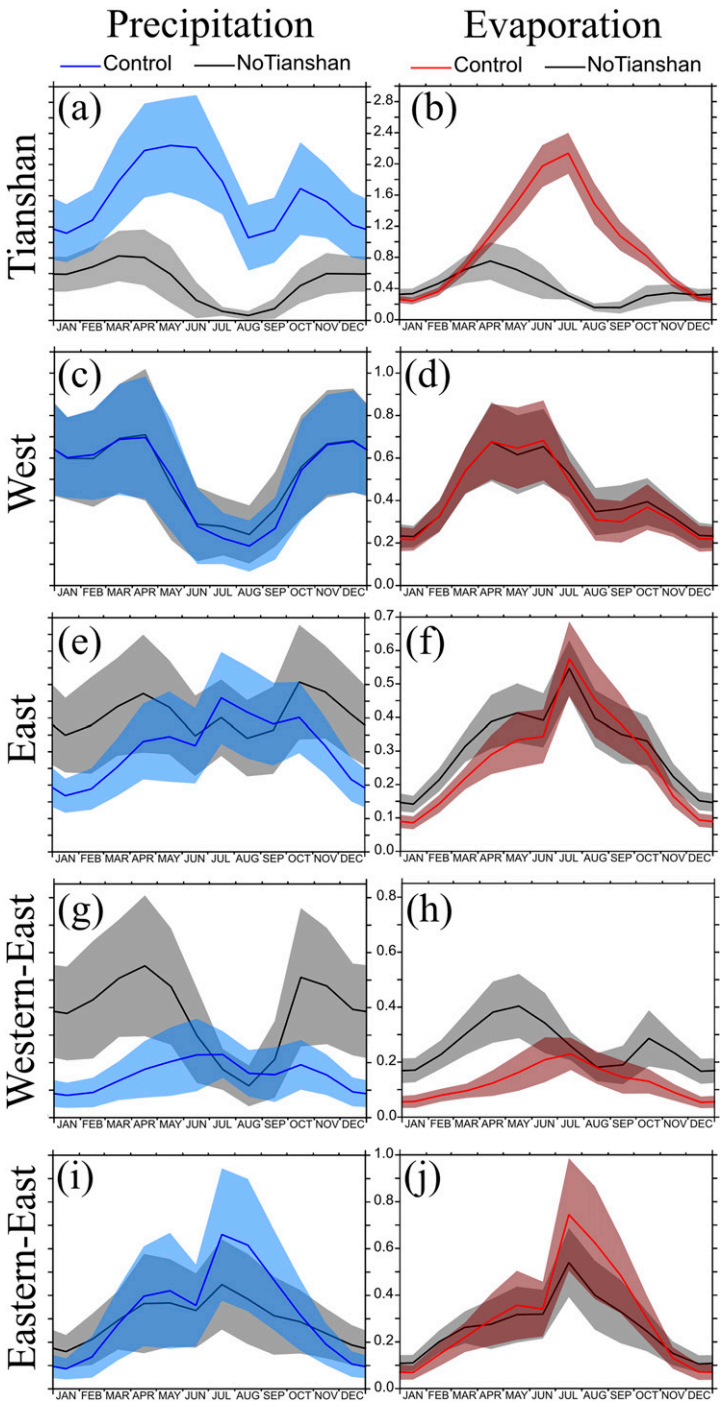

FIG. 7. Influence of the Tian Shan on seasonal cycles of different desert regions. Regional area-average seasonal cycles of (left) precipitation and (right) evaporation are plotted with one standard deviation shaded above and below curves, corresponding to different regions: (a),(b) the Tian Shan, (c),(d) the west deserts, (e),(f) the east deserts, (g),(h) the western-east region, and (i),(j) the eastern-east region. Control results are colored, and NoTianshan results are in black curves and gray shading. Averaging is done over grid cells that are desert (mean precipitation $<0.75\,\text{mm day}^{-1}$) in the Control run within the regions defined in Table 2 and shown in Fig. 3c, except for the Tian Shan region where averaging is done over grid cells that are not desert (mean precipitation $>0.75\,\text{mm day}^{-1}$). Additionally, major inland lakes and seas (such as the Caspian and Aral Seas) are excluded by averaging only over places with elevation greater than 70 m.

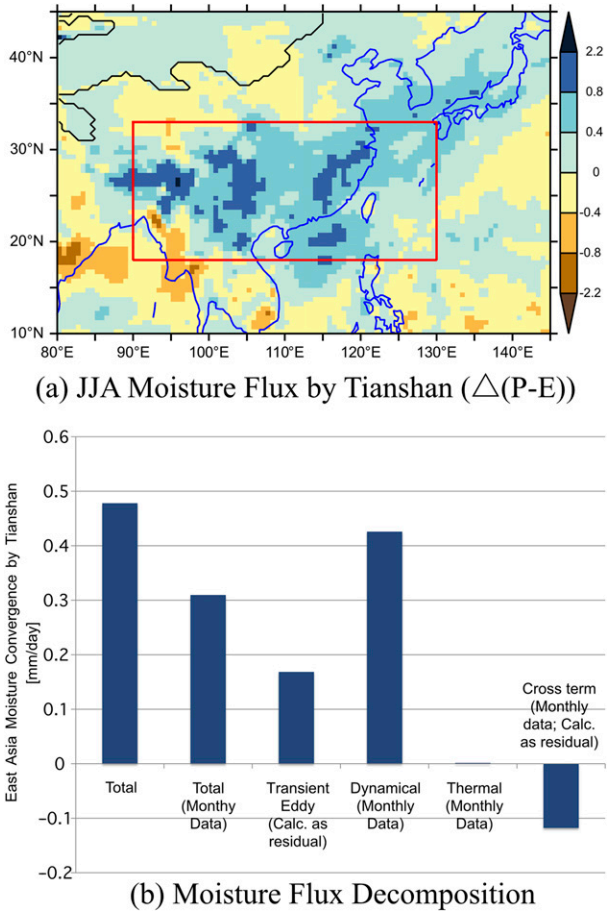

FIG. 8. Decomposition of moisture flux convergence due to the Tian Shan in East Asia. (a) Summer (JJA) Control − NoTianshan change in moisture flux convergence $[(P_{\mathrm{Cont}} - E_{\mathrm{Cont}}) - (P_{\mathrm{NoT}} - E_{\mathrm{NoT}})]$. The blue contour designates land, and the black contour designates desert. (b) Components of summer moisture flux convergence averaged over the red box in (a). Note that monthly changes account for most of the moisture convergence due to the Tian Shan, and this moisture convergence is primarily caused by dynamical (wind) not thermal (humidity) changes. See section 4a for details of this analysis.

the subscripts Cont and NoT denote Control and NoTianshan simulations, respectively} accounts for the majority (about two-thirds) of the increased moisture flux, from which we infer that about one-third comes from transient eddies. The monthly moisture flux convergence can be further separated into effects from changes in winds {dynamic effect: $-[\int_0^{p_s}\nabla\cdot(\overline{\mathbf{u}}_{\mathrm{Cont}}\overline{q}_{\mathrm{NoT}})\,dp - \int_0^{p_s}\nabla\cdot(\overline{\mathbf{u}}_{\mathrm{NoT}}\overline{q}_{\mathrm{NoT}})\,dp]$}, changes in humidity {thermal effect: $-[\int_0^{p_s}\nabla\cdot(\overline{\mathbf{u}}_{\mathrm{NoT}}\overline{q}_{\mathrm{Cont}})\,dp - \int_0^{p_s}\nabla\cdot(\overline{\mathbf{u}}_{\mathrm{NoT}}\overline{q}_{\mathrm{NoT}})\,dp]$}, and changes in correlations of the monthly wind and humidity changes {cross term: $-\int_0^{p_s}\nabla\cdot[(\overline{\mathbf{u}}_{\mathrm{Cont}} - \overline{\mathbf{u}}_{\mathrm{NoT}})(\overline{q}_{\mathrm{Cont}} - \overline{q}_{\mathrm{NoT}})]\,dp$}. Here we calculated the cross term as a residual of the monthly total, dynamic, and thermal effects (cross term is equal to monthly total minus monthly dynamic effect minus monthly thermal effect). This decomposition of monthly data indicates that dynamical effects of the Tian Shan, specifically changes in climatological mean winds and inferred changes in eddies, drive the summer moisture flux convergence over East Asia, with some divergence generated by the cross term and negligible contribution from the thermal effect.

This conclusion invites the following question: How do the Tian Shan alter climatological mean winds to drive the majority of the increased moisture flux into East Asia? Examining Control − NoTianshan change in 850-mb (1 mb = 1 hPa) moisture fluxes ($\Delta\overline{\mathbf{u}}\overline{q}$; Fig. 9), two general flows of moisture into East Asia are apparent: 1) westerly across the Arabian Sea, India, and Bay of Bengal before veering southerly around the southeast edge of the Tibetan Plateau and 2) southeasterly across southern Japan, before veering easterly and then southerly once adjacent to the Tibetan Plateau. Explaining the precipitation enhancement over East Asia requires explaining how the Tian Shan alters atmospheric circulation to force these two somewhat distinct flows.

The most prominent circulation alteration by the Tian Shan in summer is an increase in geopotential height peaking at 200 mb and just north of the Tian Shan (Fig. 10). This high is associated with a lower-atmospheric decrease in geopotential height enveloping the Tian Shan and Tibetan Plateau and a high geopotential extension farther south of this over India. Overall, this response to the Tian Shan is baroclinic throughout the atmosphere, with anticyclonic, divergent flow above and cyclonic, convergent flow below—circulation that is consistent with the response to heating in the midlatitudes predicted from potential vorticity conservation (Hoskins 1991). In the lower atmosphere, the low geopotential heights south of the Tibetan Plateau combined with high geopotential heights over India generate winds that align well with the first flow of moisture fluxes described in the previous paragraph (Fig. 10b vs Fig. 9). Thus, it seems that the lower-atmosphere cyclone associated with the Tian Shan's forced upper-atmosphere anticyclone is partially responsible for the precipitation enhancement in East Asia by the Tian Shan. It is worth noting here that certain details of the local influence by the Tian Shan on geopotential height are caused by adiabatic effects particular to the unique shape and location of the Tian Shan. For example, a particularly intense decrease in geopotential height is observed in the Tarim basin (Fig. 10), which appears to be related to the Tian Shan diverting westerly flow northward to flow through a corridor between the Tian Shan and Altai Shan before entering the Tarim basin (Fig. 11). While these local circulation changes are certainly related to the significant precipitation changes of the Tarim basin, the larger-scale baroclinic circulation response is more relevant to the remote precipitation enhancement across East Asia.

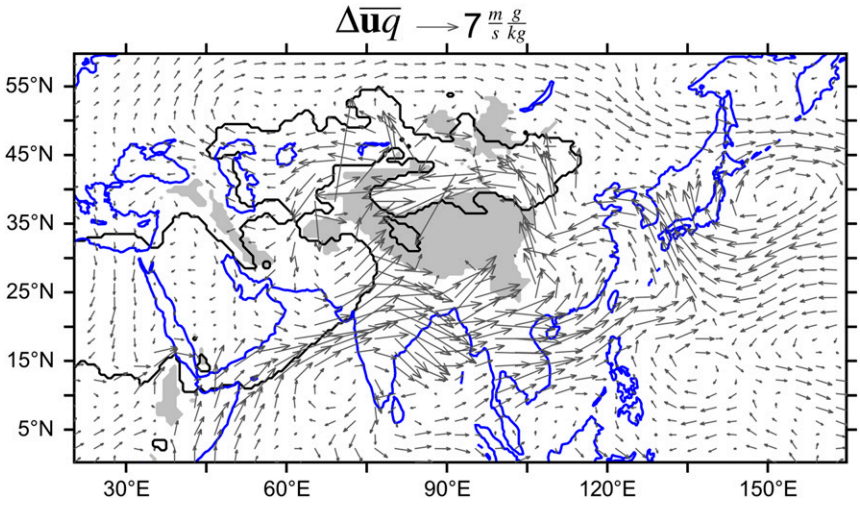

FIG. 9. Change in 850-mb JJA climatological moisture fluxes from adding in the Tian Shan $\Delta\overline{uq}$ ($m\,s^{-1}\,g\,kg^{-1}$). The black contour designates the Control desert and the blue contour designates land. Places with only topography at the relevant pressure level are masked in gray.

In addition to the baroclinic circulation change proximal to the Tibetan Plateau, examination of geopotential heights at a global scale indicates that the Tian Shan force a stationary wave that emanates eastward (Fig. 12). In the summer this wave is more significant and compact than in the winter (not shown), creating a clear anticyclone–cyclone–anticyclone pattern with the first anticyclone just northeast of the Tian Shan, the cyclone centered over northeastern China, and the second anticyclone centered just east of Japan. Unlike the first anticyclone, which is associated with a cyclone in the lower atmosphere, the circulation response associated with the cyclone and second anticyclone of the stationary wave is barotropic (not shown). Therefore, flow associated with this cyclone–anticyclone can explain the southeasterly moisture fluxes across southern Japan, which bring moisture from the Pacific and East China Sea ultimately into East Asia (Fig. 12 vs Fig. 9).

In summary, two types of mean circulation changes forced by the Tian Shan are responsible for the remote enhancement of summer precipitation in East Asia: 1) a baroclinic response typical for midlatitude forcing that generates a lower-atmosphere cyclone around the Tibetan Plateau and fluxes warm, moist air in from the southwest and 2) a barotropic stationary wave response that creates a cyclone–anticyclone pair that advects warm, moist air in from the southeast. Mountains can force circulation changes either mechanically or thermally (Held and Ting 1990). Mechanical forcing is simply the redirection of flows by the slope and elevation of the mountains. Thermal forcing is associated with orographic precipitation releasing latent heat and sensible heat flux from the elevated surface. Understanding whether the Tibetan Plateau and its constituent parts influence the Asian monsoons mechanically or thermally is a topic of extensive scientific debate (Molnar et al. 2010). While targeted experiments to address this question were outside the scope of this present work, it seems likely that the circulation and remote precipitation responses to the Tian Shan are primarily driven by thermal forcing. First, regional model experiments in Tang et al. (2013) find that elevated heating of the northern Tibetan Plateau, Tian Shan, and Altai Shan, not mechanical forcing, causes most of the enhancement of the East Asian summer monsoon by this orography. Second, dominance of thermal forcing, which peaks in the summer, would be more clearly consistent with the stationary wave being strongest in the summer than dominance of mechanical forcing. These two lines of evidence suggest that the Tian Shan's thermal forcing is more climatically influential at a large scale than its mechanical forcing.

Here we have taken one approach to diagnosing how the Tian Shan enhances precipitation in the summer over East Asia, which is consistent with prior work examining the Tibetan Plateau influence on the East Asian summer monsoon. The upper-atmosphere anticyclone and lower-atmosphere cyclone around the Tibetan Plateau have been associated in prior work with forcing by the northern Tibetan Plateau and related northern orography including the Tian Shan (Tang et al. 2013; Zhang et al. 2012; Liu et al. 2015). Additionally, the enhancement of the western North Pacific high due to the northern Tibetan Plateau is described in Zhang et al. (2012). The present study, which combines a GCM at high resolution with a specific focus on the Tian Shan,

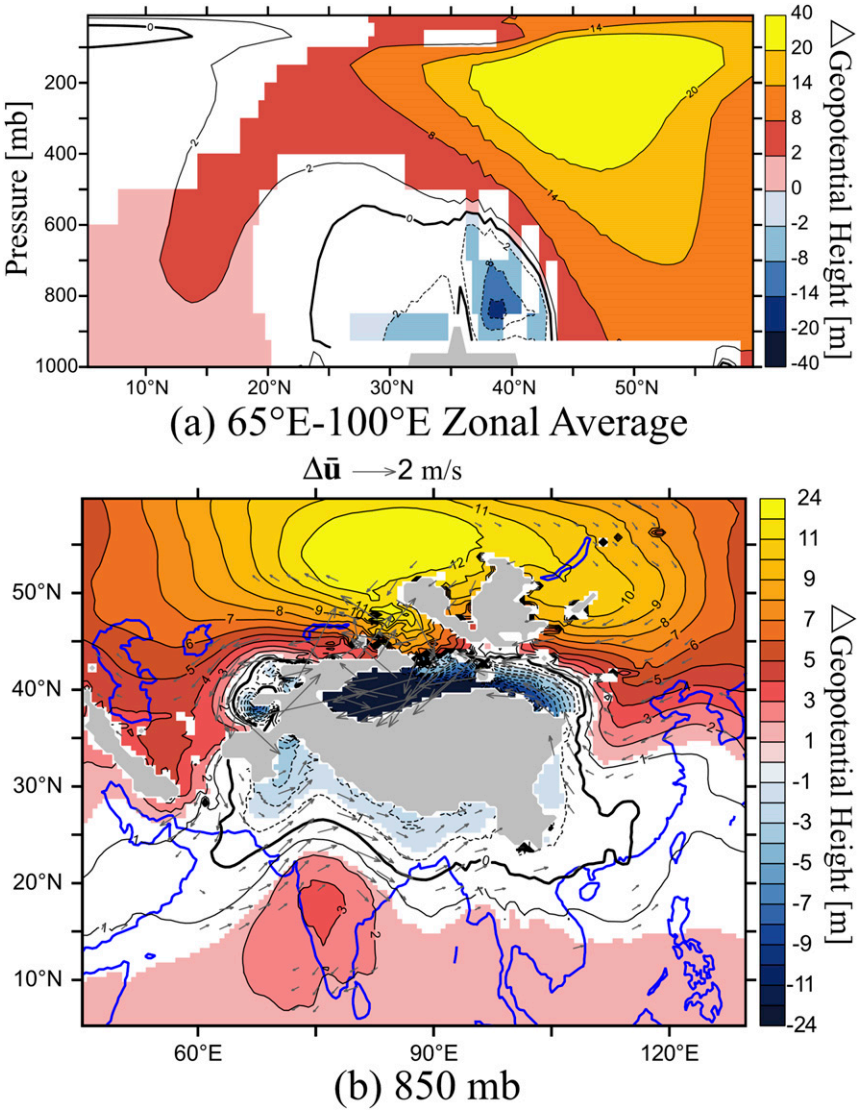

FIG. 10. The Tian Shan's influence on geopotential height and wind in summer (JJA). Shown are (a) anomalies (Control − NoTianshan) in geopotential height (m) zonally averaged over 65°–100°E and (b) anomalies in 850-mb geopotential height overlaid with wind anomaly vectors ($\Delta\bar{\mathbf{u}}$; m s^{-1}). All anomalies are contoured in black, but only significant anomalies are shaded, and places with only topography at the relevant pressure level are masked in gray. Note the baroclinic structure in (a) and south of the Tibetan Plateau the correspondence between wind vectors and the zero-anomaly contour of geopotential height in (b) with moisture flux vectors shown in Fig. 9.

has allowed clearer association of these circulation effects with the Tian Shan in particular, including diagnosis of the enhanced Pacific high as part of a stationary wave.

It is worth noting that an alternative and perhaps complementary way of examining these circulation changes is in how the Tian Shan shift the westerlies and in turn how this affects the seasonality of the East Asian summer monsoon. Chiang et al. (2015) suggest that when the westerlies shift north of the Tibetan Plateau earlier in the season, this results in longer and overall greater East Asian summer monsoon rains. Examination of the westerly jet and seasonality of East Asian monsoon precipitation in the Control and NoTianshan runs (not shown) suggests that the Tian Shan may make the westerly jet extend farther north and that the greatest enhancement of rainfall relative to the mean occurs over the farthest-north portion of the monsoon.

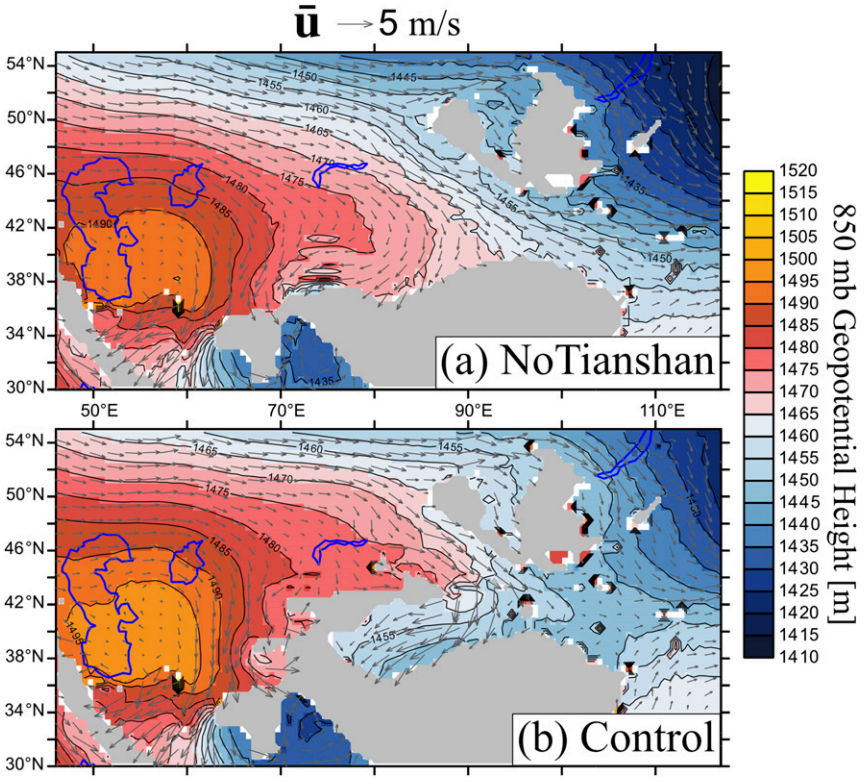

FIG. 11. Mean 850-mb geopotential height (m) and wind vectors (m s^{-1}) in summer (JJA) for (a) NoTianshan and (b) Control. Note the blocking of westerly flow by the Tian Shan and the corresponding difference in geopotential height in the lee of the Tian Shan (the western-east region).

These results are suggestive of dynamics similar to those proposed in Chiang et al. (2015). Additionally, further focus on westerly shifts may help explain eastward extension of the Tian Shan's enhancement of rainfall into the Pacific that echoes the mei-yu–baiu rainband (Fig. 6c; Sampe and Xie 2010). However, fully understanding the Tian Shan's influence in this alternative framework would require careful diagnosis of the East

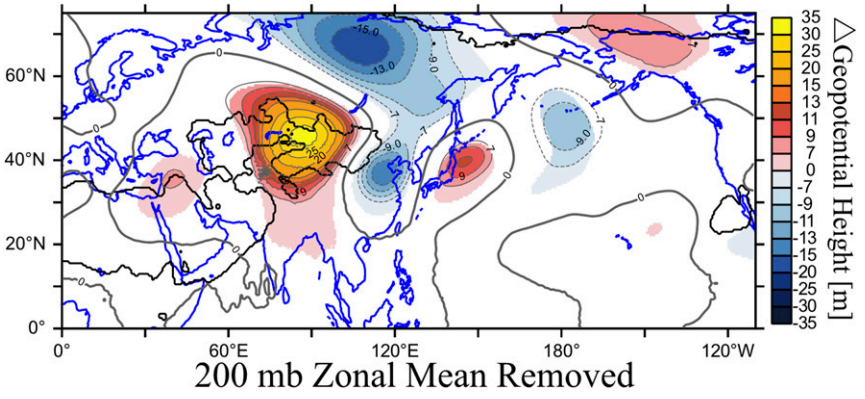

FIG. 12. The Tian Shan's stationary wave in summer (JJA). Shown are Control − NoTianshan differences in 200-mb geopotential height (m) with the zonal mean removed. All anomalies are contoured in gray, but only significant anomalies are shaded. The black contour designates desert and the blue contour designates land. Note that circulation corresponding to the low–high (cyclone–anticyclone) pattern over East Asia explains the flux of moisture from the Pacific Ocean and East China Sea into this region (seen in Fig. 9).

Asian monsoon seasonality in FLOR, which we leave to future work.

b. Temperature in AEA

In addition to influencing precipitation, the Tian Shan also generate large local surface temperature changes. There is significant cooling over the Tian Shan of up to 32°C, which can be easily explained by adiabatic cooling due to the increase in elevation. More surprisingly, there is warming of up to 5°C in the rain shadow of the Tian Shan collocated with the peaks of the Altai and Kunlun Shan (Fig. 13a).

Close inspection indicates two possible causes for this warming, both related to the blocking of winter to spring moisture from the west by the Tian Shan. One possibility is that decreased snowfall over the Altai and Kunlun Shan decreases the surface albedo and increases absorption of shortwave radiation. Snowfall does indeed decrease and absorbed shortwave radiation increases over the Altai and Kunlun Shan, consistent with this first explanation (Fig. 13b). Another possibility is that decreased soil moisture over the Altai and Kunlun Shan might decrease the potential latent heat flux and thus necessitate an increase in sensible heat flux and temperature to maintain energy balance. The Bowen ratio (sensible heat flux divided by latent heat flux) does increase over these same mountains, seemingly consistent with the second explanation for the warming (Fig. 13c).

To determine which of these two effects dominates, an energy balance decomposition was completed (Figs. 14a,b). For Control − NoTianshan, the increases in absorbed shortwave radiation over the Altai and Kunlun Shan (+13.3 and +20 $W m^{-2}$, respectively) are many times greater than the decreases in latent heat flux (+2.2 and +5.4 $W m^{-2}$, respectively). Additionally, the magnitudes of the changes in sensible heat flux (−6.6 and −12.6 $W m^{-2}$ from the Altai and Kunlun Shan, respectively) are much greater than that of latent heat flux. In this circumstance, snow cover and albedo changes, which affect the shortwave radiation budget, drive the warming. The warming is maximized at the mountains in the winter because that is where and when snowfall is significant within this otherwise arid region. Somewhat counterintuitively, change in the Bowen ratio here primarily reflects warming from snow and albedo changes driving sensible heat flux increase rather than latent heat flux decrease necessitating sensible heat flux increase. Supporting this result, the remote warming has a clear seasonality peaking in winter, when snowfall and reduction in snowfall by the Tian Shan is greatest (not shown).

A contrasting case occurs in India, which warms slightly (up to 1°C) as a result of the Tian Shan. In this warm region where there is little snow, latent heat flux does indeed drive the warming due to less precipitation (Fig. 14c). Apparently the background climate of a region (especially how much snow it receives) dictates the dominant mechanism through which drying generates warming (either decrease in snowpack and albedo as occurs in the Altai and Kunlun Shan or decrease in latent heat flux and increase in sensible heat flux as occurs in India).

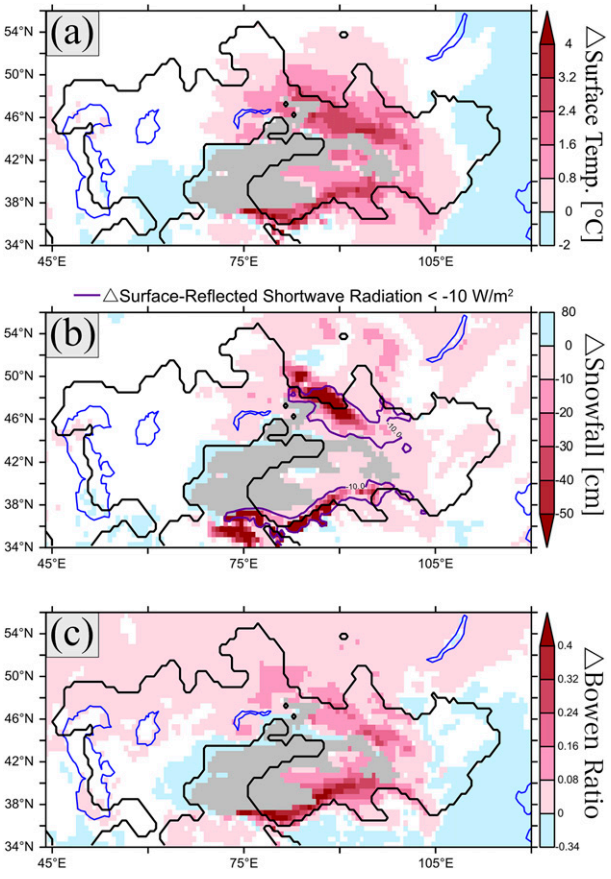

FIG. 13. Remote warming by the Tian Shan and possible mechanisms. Shown are Control − NoTianshan changes in (a) surface temperature (°C), (b) snowfall (cm) and shortwave radiation reflected from the surface (purple contour is $\Delta < -10\,W m^{-2}$), and (c) Bowen ratio. All shaded quantities are significant. The Tian Shan are masked out in light gray to highlight effects remote from the Tian Shan. The black contour designates the Control desert, and the blue contours designate lakes or seas. Note that the greatest changes in each quantity are collocated with mountains east of the Tian Shan (Altai Shan in the north and Kunlun Shan in the south).

5. Summary and discussion

This study sought to characterize the influence of the Tian Shan on arid extratropical Asia (AEA). In particular, we wanted to understand the extent to which the

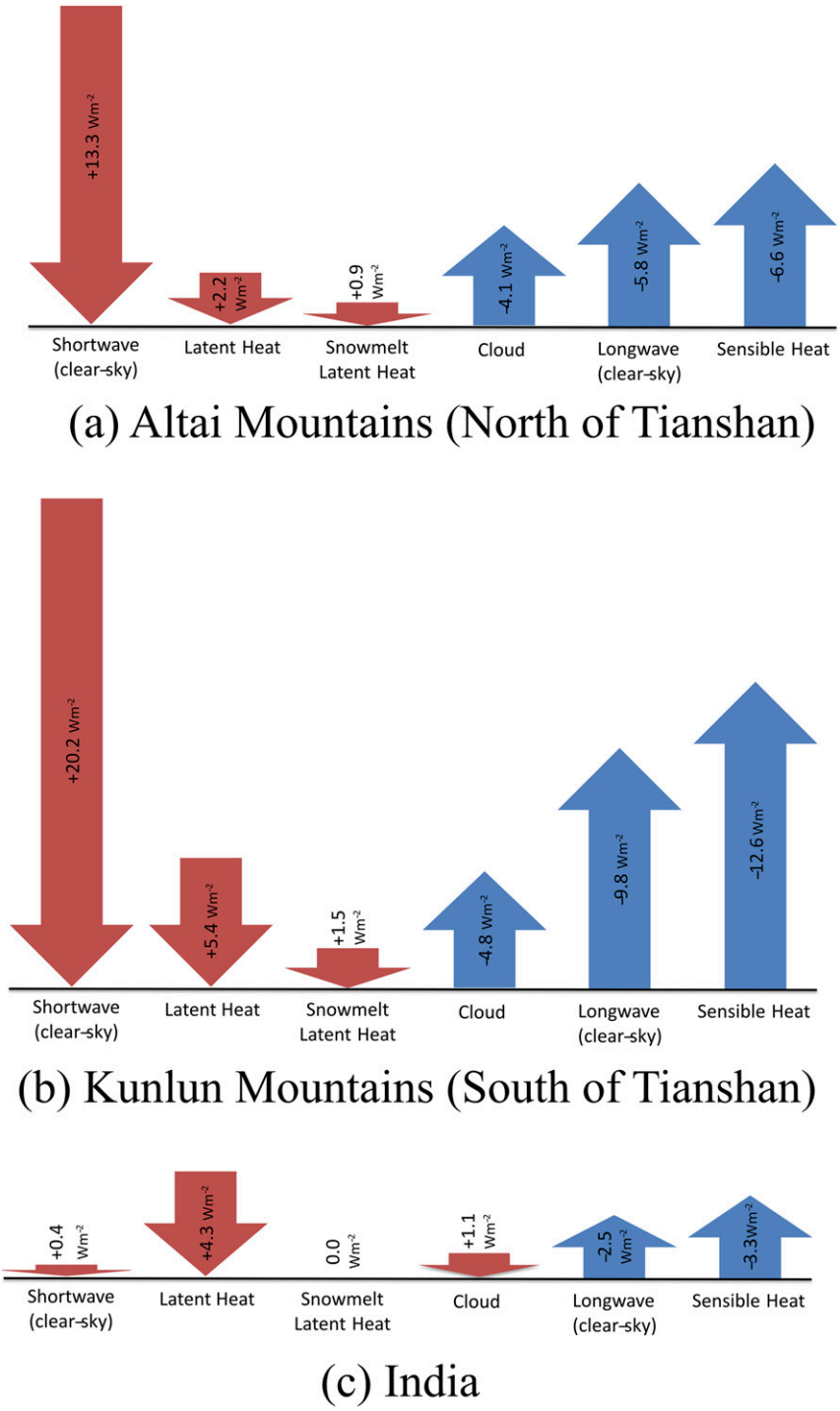

FIG. 14. Control − NoTianshan changes in the surface energy balance ($W\,m^{-2}$) for three different regions: (a) the Altai Shan, defined as mountain areas directly north of the Tian Shan that warm by more than 2°C, (b) the Kunlun Shan, defined as mountain areas directly south of the Tian Shan that warm by more than 2°C, and (c) places in India that warm by more than 0.4°C. Cloud is the change in surface radiative forcing (both shortwave and longwave) due to changes in clouds. Positive forcing implies greater energy into the surface, while negative implies greater energy leaving the surface. Note that clear-sky shortwave radiation dominates energy balance change in the mountains directly north and south of the Tian Shan, while latent heat flux dominates energy balance change in India.

Tian Shan are responsible for a wet region bisecting AEA and for the different precipitation seasonalities in the west versus east deserts. To conduct this study, we employed a newly developed high-resolution land, low-resolution ocean GFDL GCM called FLOR, which skillfully represents both the area and seasonality gradient of AEA. This model was altered to assess the impacts of the Tian Shan through three different experiments: a Control run including the Tian Shan; a NoTianshan run with boundary conditions controlling surface height, gravity wave drag, and boundary layer roughness altered to remove the Tian Shan; and a NoTianshanDrag run with boundary conditions controlling only gravity wave drag and boundary layer roughness altered to remove the Tian Shan.

The Tian Shan were found to be fully responsible for the spatial divide between the annual mean deserts and influential in important details of the seasonality differentiation. The wet region dividing the west and east deserts can be entirely attributed to orographic precipitation from the Tian Shan—the humidity in this region is likely too low for significant precipitation to occur without adiabatic lifting by the mountain slope and resulting cooling.

More interesting than the changes to desert area are the changes to desert precipitation seasonality. While the Tian Shan have negligible influence on the precipitation seasonality of the west deserts, including the Kyzyl Kum and Kara-Kum, the Tian Shan significantly alter the seasonality of precipitation in the east deserts. Normally, the driest portion of AEA known as the Taklimakan Desert (and western-east region in our study) has a weak summer peak in precipitation. When the Tian Shan are removed this region becomes much wetter, and the climatology completely switches to a fall and spring precipitation double peak as a result of three effects: 1) the westerly carried winter–spring precipitation no longer being blocked by the Tian Shan, 2) the reduced drying winter subsidence over this region in the lee of the Tian Shan, and 3) the absence of Tian Shan orographic precipitation bleeding into the region in the summer. Notably, this dramatic influence over the western-east region is consistent with paleoclimatic proxy evidence implicating the uplift by the Tian Shan in the formation of the Taklimakan Desert (Zheng et al. 2015).

The Gobi Desert or eastern-east region also receives more winter precipitation and less summer precipitation in the absence of the Tian Shan, although the change is less significant as a summer precipitation peak is retained. The causes of the change in summer precipitation in this region are not immediately obvious as it is too far from the Tian Shan to be influenced by orographic precipitation. We found through moisture budget analysis that changes in seasonal mean winds are primarily responsible for the precipitation enhancement in East Asia by the Tian Shan. The relevant circulation changes appear to be an upper-atmosphere anticyclone that is associated with a lower-atmosphere cyclone around the Tibetan Plateau and a stationary wave, both of which in turn increase moisture flux into East Asia from the west and east, respectively. This change constitutes a significant enhancement of the spring–fall East Asian monsoon and corresponds with similar results found in prior studies examining the climatic influence of the northern Tibetan Plateau, Tian Shan, and Altai Shan together (Tang et al. 2013; Zhang et al. 2012; Liu et al. 2015). Interestingly, the timing of the Tian Shan's monsoon enhancement is different from that of the Tibetan Plateau's overall influence, which Liu and Yin (2002) found to have a more significant effect on the winter than summer East Asian monsoon. Speculatively, it seems likely that these timing differences are related to the different latitudes of the Tian Shan and Tibetan Plateau paired with the seasonal meridional migration of the westerly jet.

In our simulations, changes to precipitation as a result of the Tian Shan were paired with a few temperature changes of note. The Tian Shan were found to remotely warm the Altai and Kunlun Shan to their east as follows: the Tian Shan block western winter moisture from this region, reducing orographic precipitation over the Altai and Kunlun Shan, decreasing snowpack, decreasing surface albedo, and in turn allowing greater shortwave radiation to warm the surface. This is contrasted with slight remote warming over India also related to precipitation decreases but caused proximally by Bowen ratio increase (less latent and more sensible heat fluxes).

To summarize, even without the Tian Shan, AEA is still arid, consistent with Sato (2005), and there is still a gradient in precipitation seasonality from the west to the east deserts. This suggests that large-scale circulation, separate from the influence of the Tian Shan, drives the existence and precipitation–evaporation seasonality of AEA. However, the positioning of the seasonality border between the winter–spring-dominated (west) and summer-dominated (east) deserts is strongly influenced by the Tian Shan. The Tian Shan block winter–spring precipitation from reaching the Taklimakan Desert, leading it to exist in the present climate as a summer precipitation desert more similar in seasonality to the Gobi Desert than the Kyzyl Kum and Kara-Kum. The Tian Shan also remotely enhance the summer precipitation peak in the Gobi Desert and decrease the winter precipitation. This suggests that the climatological divide of the deserts is shifted farther west and made

more distinct by the Tian Shan than it would be under the influence of moisture recycling limits alone.

There are a number of remaining questions in this study that merit further investigation. First, satellite- and ground-based observations in this region that generate the gridded observational datasets are quite sparse. Comparison of the FLOR model runs to additional observational data, such as eddy flux tower and weather station data not included in this paper's analyzed datasets, could be useful in better understanding the biases of this model in simulating AEA. Second, vegetation is static in our simulations, when in reality it likely should change when the Tian Shan are removed. Changing the vegetation to reflect the surrounding lower-elevation landscape in the NoTianshan and NoTianshanDrag runs, or rerunning these experiments with a dynamical vegetation model, would be useful additions to this work; indeed, modeling experiments by Liu et al. (2015) suggest that climate feedbacks from Taklimakan Desert formation had a comparable drying effect to the northern Tibetan Plateau (including the Tian Shan) over the Tarim basin. Additionally, in our experiments the Tian Shan create significant drying to their south and north that was not so relevant to the region of focus in this study (AEA) but may be interesting to deconstruct. Finally, how the Tian Shan forces its associated circulation changes (mechanically or thermally) and whether these changes are best considered through the frame of shifting the westerlies are important questions that merit more targeted experiments and investigation.

In recent years, AEA has seen a number of significant hydrological trends. Over the past half century, the area of China covered in desert has expanded by about $300\,km^2\,yr^{-1}$, or about 30% total (Zhang et al. 2003), and the Aral Sea in central Asia has desiccated to less than half its former size (Shibuo et al. 2007). Alongside these present trends, there is little consensus regarding how AEA will be affected by projected global warming (IPCC 2013). Future studies should work to discern to what degree proposed larger-scale climatological controls (i.e., monsoons, moisture recycling limits, and the Tibetan Plateau) are responsible for the existence and precipitation seasonality of AEA. Improved understanding of the basic climate of AEA will provide a foundation for the understanding of past, present, and future hydrological trends in these environmentally sensitive arid regions, which is of primary societal significance.

Acknowledgments. CMAP, GPCP, and University of Delaware precipitation data provided by the NOAA/OAR/ESRL Physical Sciences Division, Boulder, Colorado, from their website (http://www.esrl.noaa.gov/psd/). University of East Anglia data were provided by their Climate Research Unit from their website (http://www.cru.uea.ac.uk/data). We thank Thomas Delworth, Xiaosong Yang, P.C.D. Milly, and Isaac Held for helping conceptualize this project, and for useful comments and discussion. We also thank Seth Underwood for his crucial technical support. Finally, we are grateful for insightful comments from John Chiang and another anonymous reviewer. JWB was supported by the National Science Foundation Graduate Research Fellowship under Grant DGE 1148900. This work was partially supported by the NOAA Climate Program Office.

REFERENCES

Aizen, E. M., V. B. Aizen, J. M. Melack, T. Nakamura, and T. Ohta, 2001: Precipitation and atmospheric circulation patterns at mid-latitudes of Asia. *Int. J. Climatol.*, **21**, 535–556, doi:10.1002/joc.626.

Aizen, V. B., 2011: Tien Shan glaciers. *Encyclopedia of Snow, Ice and Glaciers*, V. P. Singh, P. Singh, and U. K. Haritashya, Eds., Springer, 1179–1181, doi:10.1007/978-90-481-2642-2_669.

——, and E. M. Aizen, 1996: Glaciers and snowcover in central Asia as indicators of climate change in the earth-ocean-atmosphere system. *Regional Hydrological Response to Climate Change*, J. A. A. Jones et al., Eds., GeoJournal Library, Vol. 38, Springer, 269–285, doi:10.1007/978-94-011-5676-9_15.

——, and ——, 1997: Hydrological cycles on the north and south peripheries of mountain glacial basins of central Asia. *Hydrol. Processes*, **11**, 451–469, doi:10.1002/(SICI)1099-1085(199704)11:5<451::AID-HYP448>3.0.CO;2-M.

——, ——, J. Melack, and T. Martma, 1996: Isotopic measurements of precipitation on central Asian glaciers (southeastern Tibet, northern Himalayas, central Tien Shan). *J. Geophys. Res.*, **101**, 9185–9196, doi:10.1029/96JD00061.

——, ——, ——, and J. Dozier, 1997: Climatic and hydrologic changes in the Tien Shan, central Asia. *J. Climate*, **10**, 1393–1404, doi:10.1175/1520-0442(1997)010<1393:CAHCIT>2.0.CO;2.

——, ——, D. R. Joswiak, K. Fujita, N. Takeuchi, and S. A. Nikitin, 2006: Climatic and atmospheric circulation pattern variability from ice-core isotope/geochemistry records (Altai, Tien Shan and Tibet). *Ann. Glaciol.*, **43**, 49–60, doi:10.3189/172756406781812078.

——, ——, and V. A. Kuzmichenok, 2007a: Geo-informational simulation of possible changes in central Asian water resources. *Global Planet. Change*, **56**, 341–358, doi:10.1016/j.gloplacha.2006.07.020.

——, ——, and V. A. Kuzmichonok, 2007b: Glaciers and hydrological changes in the Tien Shan: Simulation and prediction. *Environ. Res. Lett.*, **2**, 045019, doi:10.1088/1748-9326/2/4/045019.

Araguás-Araguás, L., K. Froehlich, and K. Rozanski, 1998: Stable isotope composition of precipitation over Southeast Asia. *J. Geophys. Res.*, **103**, 28 721–28 742, doi:10.1029/98JD02582.

Bai, Y., J. Wu, Q. Xing, Q. Pan, J. Huang, D. Yang, and X. Han, 2008: Primary production and rain use efficiency across a precipitation gradient on the Mongolia Plateau. *Ecology*, **89**, 2140–2153, doi:10.1890/07-0992.1.

Barnes, E. A., P. W. Keys, R. J. van der Ent, and L. J. Gordon, 2014: Variability of moisture recycling using a precipitationshed framework. *Hydrol. Earth Syst. Sci.*, **18**, 3937–3950, doi:10.5194/hess-18-3937-2014.

Bobojonov, I., and A. Aw-Hassan, 2014: Impacts of climate change on farm income security in central Asia: An integrated modeling approach. *Agric. Ecosyst. Environ.*, **188**, 245–255, doi:10.1016/j.agee.2014.02.033.

Bolvin, D., 2012: GPCP version 2.2 combined precipitation data set. NOAA/OAR/ESRL PSD, accessed June 2013. [Available online at http://www.esrl.noaa.gov/psd/data/gridded/data.gpcp.html.]

Boos, W. R., and J. V. Hurley, 2013: Thermodynamic bias in the multimodel mean boreal summer monsoon. *J. Climate*, **26**, 2279–2287, doi:10.1175/JCLI-D-12-00493.1.

Bosboom, R., and Coauthors, 2014: Linking Tarim Basin sea retreat (west China) and Asian aridification in the late Eocene. *Basin Res.*, **26**, 621–640, doi:10.1111/bre.12054.

Broccoli, A. J., and S. Manabe, 1992: The effects of orography on midlatitude Northern Hemisphere dry climates. *J. Climate*, **5**, 1181–1201, doi:10.1175/1520-0442(1992)005<1181:TEOOOM>2.0.CO;2.

Charney, J. G., 1975: Dynamics of deserts and drought in the Sahel. *Quart. J. Roy. Meteor. Soc.*, **101**, 193–202, doi:10.1002/qj.49710142802.

Chen, F., and Coauthors, 2008: Holocene moisture evolution in arid central Asia and its out-of-phase relationship with Asian monsoon history. *Quat. Sci. Rev.*, **27**, 351–364, doi:10.1016/j.quascirev.2007.10.017.

——, and Coauthors, 2010: Moisture changes over the last millennium in arid central Asia: A review, synthesis and comparison with monsoon region. *Quat. Sci. Rev.*, **29**, 1055–1068, doi:10.1016/j.quascirev.2010.01.005.

Cherchi, A., H. Annamalai, S. Masina, and A. Navarra, 2014: South Asian summer monsoon and the eastern Mediterranean climate: The monsoon–desert mechanism in CMIP5 simulations. *J. Climate*, **27**, 6877–6903, doi:10.1175/JCLI-D-13-00530.1.

Chiang, J. C. H., and Coauthors, 2015: Role of seasonal transitions and westerly jets in East Asian paleoclimate. *Quat. Sci. Rev.*, **108**, 111–129, doi:10.1016/j.quascirev.2014.11.009.

Delworth, T. L., and Coauthors, 2012: Simulated climate and climate change in the GFDL CM2.5 high-resolution coupled climate model. *J. Climate*, **25**, 2755–2781, doi:10.1175/JCLI-D-11-00316.1.

Dietz, A. J., C. Conrad, C. Kuenzer, G. Gesell, and S. Dech, 2014: Identifying changing snow cover characteristics in central Asia between 1986 and 2014 from remote sensing data. *Remote Sens.*, **6**, 12 752–12 775, doi:10.3390/rs61212752.

Do, N., and S. Kang, 2014: Assessing drought vulnerability using soil moisture-based water use efficiency measurements obtained from multi-sensor satellite data in northeast Asia dryland regions. *J. Arid Environ.*, **105**, 22–32, doi:10.1016/j.jaridenv.2014.02.018.

D'Odorico, P., A. Bhattachan, K. F. Davis, S. Ravi, and C. W. Runyan, 2013: Global desertification: Drivers and feedbacks. *Adv. Water Res.*, **51**, 326–344, doi:10.1016/j.advwatres.2012.01.013.

Dupont-Nivet, G., W. Krijgsman, C. G. Langereis, H. A. Abels, S. Dai, and X. Fang, 2007: Tibetan Plateau aridification linked to global cooling at the Eocene–Oligocene transition. *Nature*, **445**, 635–638, doi:10.1038/nature05516.

ECMWF, 2009: ERA-Interim project. National Center for Atmospheric Research Computational and Information Systems Laboratory Research Data Archive, accessed June 2013, doi:10.5065/D6CR5RD9.

Elguindi, N., and F. Giorgi, 2006: Simulating multi-decadal variability of Caspian Sea level changes using regional climate model outputs. *Climate Dyn.*, **26**, 167–181, doi:10.1007/s00382-005-0077-5.

Giorgi, F., J. W. Hurrell, M. R. Marinucci, and M. Beniston, 1997: Elevation dependency of the surface climate change signal: A model study. *J. Climate*, **10**, 288–296, doi:10.1175/1520-0442(1997)010<0288:EDOTSC>2.0.CO;2.

Glantz, M. H., 2005: Water, climate, and development issues in the Amu Darya basin. *Mitig. Adapt. Strategies Global Change*, **10**, 23–50, doi:10.1007/s11027-005-7829-8.

Gnanadesikan, A., and R. J. Stouffer, 2006: Diagnosing atmosphere-ocean general circulation model errors relevant to the terrestrial biosphere using the Köppen climate classification. *Geophys. Res. Lett.*, **33**, L22701, doi:10.1029/2006GL028098.

Groisman, P. Ya., and Coauthors, 2009: The Northern Eurasia Earth Science Partnership: An example of science applied to societal needs. *Bull. Amer. Meteor. Soc.*, **90**, 671–688, doi:10.1175/2008BAMS2556.1.

Guo, Z. T., and Coauthors, 2002: Onset of Asian desertification by 22myr ago inferred from loess deposits in China. *Nature*, **416**, 159–163, doi:10.1038/416159a.

Hagg, W., L. N. Braun, M. Kuhn, and T. I. Nesgaard, 2007: Modelling of hydrological response to climate change in glacierized central Asian catchments. *J. Hydrol.*, **332**, 40–53, doi:10.1016/j.jhydrol.2006.06.021.

Held, I. M., and M. Ting, 1990: Orographic versus thermal forcing of stationary waves: The importance of the mean low-level wind. *J. Atmos. Sci.*, **47**, 495–500, doi:10.1175/1520-0469(1990)047<0495:OVTFOS>2.0.CO;2.

Herzschuh, U., 2006: Palaeo-moisture evolution in monsoonal central Asia during the last 50,000 years. *Quat. Sci. Rev.*, **25**, 163–178, doi:10.1016/j.quascirev.2005.02.006.

Hilker, T., E. Natsagdorj, R. H. Waring, A. Lyapustin, and Y. Wang, 2014: Satellite observed widespread decline in Mongolian grasslands largely due to overgrazing. *Global Change Biol.*, **20**, 418–428, doi:10.1111/gcb.12365.

Hoskins, B. J., 1991: Towards a PV-θ view of the general circulation. *Tellus*, **43A**, 27–35, doi:10.1034/j.1600-0870.1991.t01-3-00005.x.

——, and D. J. Karoly, 1981: The steady linear response of a spherical atmosphere to thermal and orographic forcing. *J. Atmos. Sci.*, **38**, 1179–1196, doi:10.1175/1520-0469(1981)038<1179:TSLROA>2.0.CO;2.

IPCC, 2013: *Climate Change 2013: The Physical Science Basis*. Cambridge University Press, 1535 pp, doi:10.1017/CBO9781107415324.

Jia, L., and Coauthors, 2014: Improved seasonal prediction of temperature and precipitation over land in a high-resolution GFDL climate model. *J. Climate*, **28**, 2044–2062, doi:10.1175/JCLI-D-14-00112.1.

John, R., J. Chen, N. Lu, and B. Wilske, 2009: Land cover/land use change in semi-arid Inner Mongolia: 1992–2004. *Environ. Res. Lett.*, **4**, 045010, doi:10.1088/1748-9326/4/4/045010.

Jones, P., and I. Harris, 2013: University of East Anglia Climate Research Unit (CRU) TS3.21 gridded precipitation since 1901. NCAS British Atmospheric Data Centre, accessed January 2016, doi:10.5285/D0E1585D-3417-485F-87AE-4FCECF10A992.

Kreutz, K. J., C. P. Wake, V. B. Aizen, L. D. Cecil, and H.-A. Synal, 2003: Seasonal deuterium excess in a Tien Shan ice core: Influence of moisture transport and recycling in central Asia. *Geophys. Res. Lett.*, **30**, 1922, doi:10.1029/2003GL017896.

Lee, S.-S., J.-Y. Lee, K.-J. Ha, B. Wang, A. Kitoh, Y. Kajikawa, and M. Abe, 2013: Role of the Tibetan Plateau on the annual variation of mean atmospheric circulation and storm track activity. *J. Climate*, **26**, 5270–5286, doi:10.1175/JCLI-D-12-00213.1.

Li, H., and X. Yang, 2014: Temperate dryland vegetation changes under a warming climate and strong human intervention—With

a particular reference to the district Xilin Gol, Inner Mongolia, China. *Catena*, **119**, 9–20, doi:10.1016/j.catena.2014.03.003.

Linderholm, H. W., T. Ou, J.-H. Jeong, C. K. Folland, D. Gong, H. Liu, Y. Liu, and D. Chen, 2011: Interannual teleconnections between the summer North Atlantic Oscillation and the East Asian summer monsoon. *J. Geophys. Res.*, **116**, D13107, doi:10.1029/2010JD015235.

Lioubimtseva, E., and G. M. Henebry, 2009: Climate and environmental change in arid central Asia: Impacts, vulnerability, and adaptations. *J. Arid Environ.*, **73**, 963–977, doi:10.1016/j.jaridenv.2009.04.022.

——, R. Cole, J. Adams, and G. Kapustin, 2005: Impacts of climate and land-cover changes in arid lands of central Asia. *J. Arid Environ.*, **62**, 285–308, doi:10.1016/j.jaridenv.2004.11.005.

Liu, X., and Z.-Y. Yin, 2002: Sensitivity of East Asian monsoon climate to the uplift of the Tibetan Plateau. *Palaeogeogr. Palaeoclimatol. Palaeoecol.*, **183**, 223–245, doi:10.1016/S0031-0182(01)00488-6.

——, H. Sun, Y. Miao, B. Dong, and Z.-Y. Yin, 2015: Impacts of uplift of northern Tibetan Plateau and formation of Asian inland deserts on regional climate and environment. *Quat. Sci. Rev.*, **116**, 1–14, doi:10.1016/j.quascirev.2015.03.010.

Liu, Y., and Coauthors, 2014: Response of evapotranspiration and water availability to the changing climate in northern Eurasia. *Climatic Change*, **126**, 413–427, doi:10.1007/s10584-014-1234-9.

Lu, N., B. Wilske, J. Ni, R. John, and J. Chen, 2009: Climate change in Inner Mongolia from 1955 to 2005: Trends at regional, biome and local scales. *Environ. Res. Lett.*, **4**, 045006, doi:10.1088/1748-9326/4/4/045006.

Manabe, S., and T. B. Terpstra, 1974: The effects of mountains on the general circulation of the atmosphere as identified by numerical experiments. *J. Atmos. Sci.*, **31**, 3–42, doi:10.1175/1520-0469(1974)031<0003:TEOMOT>2.0.CO;2.

Matsuura, K., 2010: University of Delaware air temperature & precipitation V3.01. NOAA/OAR/ESRL PSD, accessed June 2013. [Available online at http://www.esrl.noaa.gov/psd/data/gridded/data.UDel_AirT_Precip.html.]

Micklin, P., 2007: The Aral Sea disaster. *Annu. Rev. Earth Planet. Sci.*, **35**, 47–72, doi:10.1146/annurev.earth.35.031306.140120.

Molnar, P., W. R. Boos, and D. S. Battisti, 2010: Orographic controls on climate and paleoclimate of Asia: Thermal and mechanical roles for the Tibetan Plateau. *Annu. Rev. Earth Planet. Sci.*, **38**, 77–102, doi:10.1146/annurev-earth-040809-152456.

Nagashima, K., R. Tada, and S. Toyoda, 2013: Westerly jet-East Asian summer monsoon connection during the Holocene. *Geochem. Geophys. Geosyst.*, **14**, 5041–5053, doi:10.1002/2013GC004931.

NASA GMAO, 2011: Modern Era Retrospective-Analysis for Research and Applications (MERRA). NASA Goddard Earth Science Data and Information Services Center, accessed June 2013. [Available online at http://gmao.gsfc.nasa.gov/merra/.]

NOAA/NCEP, 2012: NCEP-DOE Reanalysis 2: Summary. NOAA/OAR/ESRL PSD, accessed June 2013. [Available online at http://www.esrl.noaa.gov/psd/data/gridded/data.ncep.reanalysis2.html.]

Ososkova, T., N. Gorelkin, and V. Chub, 2000: Water resources of central Asia and adaptation measures for climate change. *Environ. Monit. Assess.*, **61**, 161–166, doi:10.1023/A:1006394808699.

Park, H.-S., J. C. Chiang, and S.-W. Son, 2010: The role of the central Asian mountains on the midwinter suppression of North Pacific storminess. *J. Atmos. Sci.*, **67**, 3706–3720, doi:10.1175/2010JAS3349.1.

——, ——, and S. Bordoni, 2012: The mechanical impact of the Tibetan Plateau on the seasonal evolution of the South Asian monsoon. *J. Climate*, **25**, 2394–2407, doi:10.1175/JCLI-D-11-00281.1.

Parungo, F., Z. Li, X. Li, D. Yang, and J. Harris, 1994: Gobi dust storms and the Great Green Wall. *Geophys. Res. Lett.*, **21**, 999–1002, doi:10.1029/94GL00879.

Pederson, N., and Coauthors, 2013: Three centuries of shifting hydroclimatic regimes across the Mongolian breadbasket. *Agric. For. Meteor.*, **178–179**, 10–20, doi:10.1016/j.agrformet.2012.07.003.

——, A. E. Hessl, N. Baatarbileg, K. J. Anchukaitis, and N. D. Cosmo, 2014: Pluvials, droughts, the Mongol empire, and modern Mongolia. *Proc. Natl. Acad. Sci. USA*, **111**, 4375–4379, doi:10.1073/pnas.1318677111.

Pierrehumbert, R. T., 1986: An essay on the parameterization of orographic gravity wave drag. *Proc. Seminar/Workshop on Observation, Theory and Modeling of Orographic Effects*, Reading, United Kingdom, ECMWF, 251–282.

Qian, W., L. Quan, and S. Shi, 2002: Variations of the dust storm in China and its climatic control. *J. Climate*, **15**, 1216–1229, doi:10.1175/1520-0442(2002)015<1216:VOTDSI>2.0.CO;2.

Rea, D. K., H. Snoeckx, and L. H. Joseph, 1998: Late Cenozoic eolian deposition in the North Pacific: Asian drying, Tibetan uplift, and cooling of the Northern Hemisphere. *Paleoceanography*, **13**, 215–224, doi:10.1029/98PA00123.

Rodwell, M. J., and B. J. Hoskins, 1996: Monsoons and the dynamics of deserts. *Quart. J. Roy. Meteor. Soc.*, **122**, 1385–1404, doi:10.1002/qj.49712253408.

Saiko, T. A., and I. S. Zonn, 2000: Irrigation expansion and dynamics of desertification in the circum-Aral region of central Asia. *Appl. Geogr.*, **20**, 349–367, doi:10.1016/S0143-6228(00)00014-X.

Sampe, T., and S.-P. Xie, 2010: Large-scale dynamics of the meiyu–baiu rainband: Environmental forcing by the westerly jet. *J. Climate*, **23**, 113–134, doi:10.1175/2009JCLI3128.1.

Sato, T., 2005: The Tian Shan rain-shadow influence on the arid climate formation in northwestern China. *Sola*, **1**, 13–16, doi:10.2151/sola.2005-004.

——, F. Kimura, and A. Kitoh, 2007: Projection of global warming onto regional precipitation over Mongolia using a regional climate model. *J. Hydrol.*, **333**, 144–154, doi:10.1016/j.jhydrol.2006.07.023.

Schiemann, R., D. Lüthi, and C. Schär, 2009: Seasonality and interannual variability of the westerly jet in the Tibetan Plateau region. *J. Climate*, **22**, 2940–2957, doi:10.1175/2008JCLI2625.1.

Seager, R., and G. A. Vecchi, 2010: Greenhouse warming and the 21st century hydroclimate of southwestern North America. *Proc. Natl. Acad. Sci. USA*, **107**, 21 277–21 282, doi:10.1073/pnas.0910856107.

Shibuo, Y., J. Jarsj, and G. Destouni, 2007: Hydrological responses to climate change and irrigation in the Aral Sea drainage basin. *Geophys. Res. Lett.*, **34**, L21406, doi:10.1029/2007GL031465.

Siegfried, T., T. Bernauer, R. Guiennet, S. Sellars, A. W. Robertson, J. Mankin, P. Bauer-Gottwein, and A. Yakovlev, 2012: Will climate change exacerbate water stress in central Asia? *Climatic Change*, **112**, 881–899, doi:10.1007/s10584-011-0253-z.

Small, E. E., F. Giorgi, and L. C. Sloan, 1999a: Regional climate model simulation of precipitation in central Asia: Mean and interannual variability. *J. Geophys. Res.*, **104**, 6563–6582, doi:10.1029/98JD02501.

——, L. C. Sloan, S. Hostetler, and F. Giorgi, 1999b: Simulating the water balance of the Aral Sea with a coupled regional climate-lake model. *J. Geophys. Res.*, **104**, 6583–6602, doi:10.1029/98JD02348.

Sorg, A., T. Bolch, M. Stoffel, O. Solomina, and M. Beniston, 2012: Climate change impacts on glaciers and runoff in Tien Shan (central Asia). *Nat. Climate Change*, **2**, 725–731, doi:10.1038/nclimate1592.

Sun, B., and H. Wang, 2013: Moisture sources of semi-arid grassland in China using the Lagrangian particle model FLEXPART. *J. Climate*, **27**, 2457–2474, doi:10.1175/JCLI-D-13-00517.1.

Tang, H., A. Micheels, J. T. Eronen, B. Ahrens, and M. Fortelius, 2013: Asynchronous responses of East Asian and Indian summer monsoons to mountain uplift shown by regional climate modelling experiments. *Climate Dyn.*, **40**, 1531–1549, doi:10.1007/s00382-012-1603-x.

Unger-Shayesteh, K., S. Vorogushyn, D. Farinotti, A. Gafurov, D. Duethmann, A. Mandychev, and B. Merz, 2013: What do we know about past changes in the water cycle of Central Asian headwaters? A review. *Global Planet. Change*, **110**, 4–25, doi:10.1016/j.gloplacha.2013.02.004.

van der Ent, R. J., H. H. Savenije, B. Schaefli, and S. C. Steele-Dunne, 2010: Origin and fate of atmospheric moisture over continents. *Water Resour. Res.*, **46**, W09525, doi:10.1029/2010WR009127.

Vecchi, G., and Coauthors, 2014: On the seasonal forecasting of regional tropical cyclone activity. *J. Climate*, **27**, 7994–8016, doi:10.1175/JCLI-D-14-00158.1.

Wang, B., Q. Bao, B. Hoskins, G. Wu, and Y. Liu, 2008: Tibetan Plateau warming and precipitation changes in East Asia. *Geophys. Res. Lett.*, **35**, L14702, doi:10.1029/2008GL034330.

Wang, X., Z. Dong, J. Zhang, and L. Liu, 2004: Modern dust storms in China: An overview. *J. Arid Environ.*, **58**, 559–574, doi:10.1016/j.jaridenv.2003.11.009.

——, F. Chen, and Z. Dong, 2006: The relative role of climatic and human factors in desertification in semiarid China. *Global Environ. Change*, **16**, 48–57, doi:10.1016/j.gloenvcha.2005.06.006.

Wu, G., and Coauthors, 2007: The influence of mechanical and thermal forcing by the Tibetan Plateau on Asian climate. *J. Hydrometeor.*, **8**, 770–789, doi:10.1175/JHM609.1.

Xie, P., 2012: CPC Merged Analysis of Precipitation (CMAP). NOAA/OAR/ESRL PSD, accessed June 2013. [Available online at http://www.esrl.noaa.gov/psd/data/gridded/data.cmap.html.]

Xue, Y., 1996: The impact of desertification in the Mongolian and the Inner Mongolian grassland on the regional climate. *J. Climate*, **9**, 2173–2189, doi:10.1175/1520-0442(1996)009<2173:TIODIT>2.0.CO;2.

Xuejie, G., Z. Zongci, D. Yihui, H. Ronghui, and F. Giorgi, 2001: Climate change due to greenhouse effects in China as simulated by a regional climate model. *Adv. Atmos. Sci.*, **18**, 1224–1230, doi:10.1007/s00376-001-0036-y.

Yang, X., Z. Liu, F. Zhang, P. D. White, and X. Wang, 2006: Hydrological changes and land degradation in the southern and eastern Tarim basin, Xinjiang, China. *Land Degrad. Dev.*, **17**, 381–392, doi:10.1002/ldr.744.

——, L. Scuderi, P. Paillou, Z. Liu, H. Li, and X. Ren, 2011: Quaternary environmental changes in the drylands of China: A critical review. *Quat. Sci. Rev.*, **30**, 3219–3233, doi:10.1016/j.quascirev.2011.08.009.

——, and Coauthors, 2015: Seasonal predictability of extratropical storm tracks in GFDL's high-resolution climate prediction model. *J. Climate*, **28**, 3592–3611, doi:10.1175/JCLI-D-14-00517.1.

Yatagai, A., and T. Yasunari, 1995: Interannual variations of summer precipitation in the arid/semi-arid regions in China and Mongolia: Their regionality and relation to the Asian summer monsoon. *J. Meteor. Soc. Japan*, **73**, 909–923.

——, and Coauthors, 2011: APHRODITE precipitation 0.25 × 0.25 degrees. Subsets used: Monsoon Asia, Middle East, and northern Eurasia, APHRODITE's Water Resources, accessed June 2015. [Available online at http://www.chikyu.ac.jp/precip/english/products.html.]

Yu, F., K. P. Price, J. Ellis, J. J. Feddema, and P. Shi, 2004: Interannual variations of the grassland boundaries bordering the eastern edges of the Gobi Desert in central Asia. *Int. J. Remote Sens.*, **25**, 327–346, doi:10.1080/0143116031000084297.

Zhang, R., D. Jiang, X. Liu, and Z. Tian, 2012: Modeling the climate effects of different subregional uplifts within the Himalaya-Tibetan Plateau on Asian summer monsoon evolution. *Chin. Sci. Bull.*, **57**, 4617–4626, doi:10.1007/s11434-012-5284-y.

Zhang, X. Y., S. L. Gong, T. L. Zhao, R. Arimoto, Y. Q. Wang, and Z. J. Zhou, 2003: Sources of Asian dust and role of climate change versus desertification in Asian dust emission. *Geophys. Res. Lett.*, **30**, 2272, doi:10.1029/2003GL018206.

Zheng, H., X. Wei, R. Tada, P. D. Clift, B. Wang, F. Jourdan, P. Wang, and M. He, 2015: Late Oligocene–early Miocene birth of the Taklimakan Desert. *Proc. Natl. Acad. Sci. USA*, **25**, 7662–7667, doi:10.1073/pnas.1424487112.

Zhisheng, A., J. E. Kutzbach, W. L. Prell, and S. C. Porter, 2001: Evolution of Asian monsoons and phased uplift of the Himalaya–Tibetan Plateau since late Miocene times. *Nature*, **411**, 62–66, doi:10.1038/35075035.

Zonn, I. S., and P. E. Esenov, 2012: The Karakum Desert. *The Turkmen Lake Altyn Asyr and Water Resources in Turkmenistan*, I. S. Zonn and A. G. Kostianoy, Eds., Springer, 23–37, doi:10.1007/698_2012_192.